Jacaranda Mimosifolia Waste seed pod Activated Carbon-Fe_3O_4 Nanocomposite for Removal of Methylene Blue from Synthetic Wastewater

Kebede Shimelis

A Thesis Submitted to the Department of Applied Chemistry

School of Applied Natural Science

Presented in Partial Fulfillment of the Requirements for the Degree of Master of Science in Applied Chemistry (Industrial Chemistry)

Office of Graduate Studies

Adama Science and Technology University

June, 2024
Adama, Ethiopia

Jacaranda Mimosifolia Waste seed pod Activated Carbon-Fe_3O_4 Nanocomposite for Removal of Methylene Blue from Synthetic Wastewater

Kebede Shimelis

Advisor: Fedlu Kedir (PhD)

A Thesis Submitted to the Department of Applied Chemistry

School of Applied Natural Science

Presented in Partial Fulfillment of the Requirements for the Degree of

Master of Science in Applied Chemistry (Industrial Chemistry)

Office of Graduate Studies

Adama Science and Technology University

June, 2024

Adama, Ethiopia

DECLARATION

I hereby declare that this Master Thesis entitled **"***Jacaranda Mimosifolia* Waste seed pod Activated Carbon-Fe_3O_4 Nanocomposite for Removal of Methylene Blue from Wastewater**"** is my original work. It has not been submitted for the award of any academic degree, diploma, or certificate in any other university. All sources of materials that are used for this thesis have been duly acknowledged through citation.

Name of the student	Signature	Date

RECOMMENDATION

I, the advisor of this thesis, hereby certify that I have read the revised version of the thesis entitled **“** *Jacaranda Mimosifolia* Waste seed pod Activated Carbon-Fe_3O_4 Nanocomposite for Removal of Methylene Blue from Wastewater**”** prepared under my guidance by **Kebede Shimelis** submitted in partial fulfillment of the requirements for the degree of Master of Science in Applied Chemistry (Industrial Chemistry). Therefore, I recommend the submission of revised version of the thesis to the department following the applicable procedures.

Fedlu Kedir (PhD)

Major Advisor	Signature	Date

APPROVAL SHEET

I, the advisor of the thesis entitled *Jacaranda Mimosifolia* Waste seed pod Activated Carbon-Fe_3O_4 Nanocomposite for Removal of Methylene Blue from Wastewater‖ and developed by **Kebede Shimelis Dinku**; here by certify that the recommendation and suggestions made by the board of examiners are appropriately incorporated into the final version of the thesis.

Major Supervisor	Signature	Date

We, the undersigned, members of the Board of Examiners of the thesis by Kebede Shimelis Dinku have read and evaluated the thesis entitled "*Jacaranda Mimosifolia* Waste seed pod Activated Carbon-Fe_3O_4 Nanocomposite for Removal of Methylene Blue from Wastewater" and examined the candidate during the open defense. This is, therefore, to certify that the thesis is accepted for partial fulfillment of the requirement of the degree of Master of Science in Applied Chemistry (Specialization in Industrial Chemistry).

Chairperson	Signature	Date
Internal Examiner	Signature	Date
External Examiner	Signature	Date

Finally, approval and acceptance of the thesis are contingent upon submission of its final copy to the Office of Postgraduate Studies (OPGS) through the candidate's Department Graduate Council (DGC) and School Graduate Committee (SGC).

Department Head	Signature	Date
School Dean	Signature	Date
Office of Postgraduate Studies, Dean	Signature	Date

TABLE OF CONTENTS

LIST OF FIGURES

LIST OF TABLES

LIST OF ABREVIATIONS

AC	Activated Carbon
MB	Methylene Blue
FTIR	Fourier Transform Infrared
JM	*Jacaranda Mimosifolia*
MNPs	Magnetic Nanoparticles
MAC	Magnetic Activated Carbon
NMO	Nano metal oxides
SEM	Scanning electron microscopy
TGA	Thermal gravimetric analysis
TMO	Transition-metal oxides
UV-VIS	Ultraviolet Visible Spectroscopy
USEPA	United States Environmental Protection Agency
XRD	X -Ray Diffraction

Abstract

In this study AC-Fe_3O_4 nanocomposite adsorbents were prepared and used for removal of methylene blue dye from aqueous effluents. Synthesized adsorbent samples were characterized using Fourier transform-infrared (FT-IR) spectroscopy, X-ray powder diffraction (XRD), thermo gravimetric analysis (TGA), and scanning electron microscopy (SEM). The AC-Fe_3O_4 nanocomposite adsorbents MB removal efficiency was investigated using a batch adsorption technique, and the effect of experimental parameters such as pH of the solution, contact time, initial MB concentration, and adsorbent dosage were studied carefully. Using the optimized parameters, the kinetics and adsorption isotherm as well as reusability of the adsorbents were also investigated. The result revealed that, the adsorption efficiency of the composite increased by increasing the pH of the solution, adsorbent dose and contact time, and reached maximum at pH 7, adsorbent dose of 0.1g, contact time of 15 min, initial MB dye concentration of 50 mg/L at room temperature. The mechanism of pollutant adsorption on the surface of AC-Fe_3O_4 nanocomposite was tested using adsorption kinetics and adsorption isotherms. The regenerability of the adsorbent was also evaluated for six cycles. From the prepared samples AC-Fe_3O_4 nanocomposite, 2:1 ratio showed maximum removal efficiency of 99.98%, maximum adsorption capacity of 49.94 mg/g for MB, and the adsorbent has shown excellent reusability for six cycles without drastic change in its property. The kinetics of the adsorption process fitted well with the Pseudo-second-order kinetic model and from the tested isotherm model, the Langmuir isotherm model was found to be the best fit. From the regeneration study, it is possible to conclude that AC-Fe_3O_4 nanocomposite was recyclable and reused as MB dye adsorption for 6 successive cycles without significant efficiency loss.

Keywords: *Jacaranda Mimosifolia*, Activated carbon, AC-Fe_3O_4 nanocomposite, Methylene blue, Adsorptive removal, Industrial wastewater

1. INTRODUCTION

1.1. Background of Study

The severe water contaminations by natural and anthropogenic causes have become one of the major environmental challenges of the 21st century. More than 2000 chemical pollutants, mostly organic pollutants, have been discovered in wastewater (Mironyuk et al., 2019). Organic dyes, widely employed in a variety of areas, are among the organic contaminants that cause substantial water pollution. Among the different types of organic dyes, Methylene blue (MB), a cationic thiazide redox dye, is abundant in wastewater and surface water due to its use in several industries. It contains a lot of organic groups, such as phenyl and amino groups, and has a complex structure. It is stable and difficult to degrade after entering the water bodies (Y. Qiu et al., 2009).

Even though MB is essential and widely used in many industries, excessive discharge of it from various sources into aquatic systems is a matter of concern because of its toxic, mutagenic or carcinogenic properties (Markandeya. et al., 2017). Due to its hostility, it will cause serious adverse effects on the environment and human health. As a result, Environmental Protection Agency (EPA) recommends a limit value of 0.2 mg/L of MB in wastewater (Environmental Protection Agency, 2001). For that reason, treating MB effluent before discharging it into the environment is critical in order to meet the EPA limit and for limiting its negative effects. Among the different MB dye removal methods from contaminated water, adsorption is one of the most often utilized methods in dye wastewater remediation and it is quite effective for removing dyes in water (Bulgariu et al., 2019). However, commercial adsorbent materials are both very expensive and non-renewable, which limits their practical utility. To address this issue, production of low-cost adsorbent material from locally available resources such as activated carbon (AC), have been investigated (Bagheri et al., 2017, Xiaoduo Liu et al., 2019).

AC refers to a group of carbon materials with high oscillation and high internal surface which are unique because of their remarkable interior area, pore structure, high adsorption capacity, surface reactivity and low cost compared to inorganic adsorbents such as zeolite (Rahimian et al., 2020). AC is one of the best adsorbents which is widely used because of its excellent porosity, low density as well as high adsorption capacity towards various organic compounds (Angin et al., 2014). AC can be obtained from various agricultural wastes and by-products,

which have received significant attention as they are low-cost, renewable and environmentally friendly Recently, several types of ACs were obtained using bamboo (Zhao et al., 2016), coconut shell (Aljeboree *et al.*, 2017), etc. as raw materials. It is proven that agricultural biomasses can be used to produce activated carbon for the removal of different types of pollutants (Zabi *et al*., 2021).

Ultimately, adsorption onto AC is a well-established and cost-effective technique among the various treatment processes because of its simplicity in design, ease of operation, and high adsorption capacity (Vunain et al., 2017, Xiaoduo Liu et al., 2019). For example, Lignocellulosic precursors obtained from crops and fruits offer several advantages for synthesizing activated carbons due to its wide availability and their interesting physicochemical properties. Particularly, biomass of jacaranda is alternative lignocellulosic precursors for activated carbon preparation (Cordero *et al*, 2013). Jacaranda is a flowering plant commonly found in Ethiopia, its fruits are dense, rounded, and woody in the form of capsules. They are produced in large volumes, and when ripen; open, releasing the seeds as waste. The use of waste materials for the preparation of AC is also very attractive from the point of view of their contribution to decrease the costs of waste disposal, therefore is used to help environmental protection (Pathania et al., 2017).

The adsorption efficiency of AC derived from Jacaranda Mimosifolia (JM) can be improved by adopting various activation processes. The most commonly used activation methods are physical activation and chemical activation. Several studies reported that adding or mixing additives (surfactants, metals, catalysts, agriculture based residues and industry waste) in the fresh AC or after carbonization, enhanced the adsorption capacity(Bagheri et al., 2017). Aside from these modifications, to further increase the methylene blue (MB) adsorption capacity of AC, forming a composite adsorbent is a promising approach due to the chemical nature, high surface area, and amorphous structure of the AC. However, it has the problems to separate them from water body, causing the secondary pollution. Meanwhile, non-recyclability is cost ineffective and may limit the applications of pure AC materials on a large scale in many fields.

Magnetic separation is a renewable recycling technology applied widely in physics, chemistry, and other separation processes, such as tissue repair, magnetic resonance imaging, drug delivery, molecular diagnostics, and catalysis, because of its fast and noncontact

magnetic response. Therefore, the magnetically functionalized carbon materials have gained extensive attention in the purification of water (Y. Zhang et al., 2011, Yu et al., 2013). For example, a magnetic multiwall carbon nanotube was prepared for removing cationic dyes from aqueous solution(Gong et al., 2009), 2D- carbon flakes and Fe_3O_4 nanoparticles were used to remove As(III) ions from wastewater (Venkateswarlu et al., 2016). However, these reported magnetically functionalized carbon materials were still unsatisfactory in keeping both high adsorption capacity and rapid magnetic separation(Bagheri et al., 2017, Xiaoduo Liu et al., 2019).

Herein, we focused on enhancing the adsorption capacity and the adsorption mechanisms using Fe_3O_4 magnetic nanoparticles entrapped with AC (AC-Fe_3O_4) composite as an adsorbent to MB, the typical dyes, from the aqueous solution.

1.2. Statement of the Problem

Dyeing industry effluents constitute one of the most problematic wastewaters to be treated not only for their high chemical and biological oxygen demands, suspended solids, and content in toxic compounds but also for colour, which are the first contaminant to be recognized by the human eye (Karaer et al., 2016). Industries that utilize MB dye for dyeing purpose produce MB contaminated wastewater, resulting high risks to public health, the surrounding environment and socioeconomic activities. This is because of its non-biodegradability as exhibited by its stability against sunlight, temperature, oxidizing agents, and microbial attack (Hassaan et al., 2017, Sham et al., 2018). Thus, dye wastewater needs to be treated for the sake of the protection of human health and environmental safety (Gao et *al*., 2013).

Different conventional methods were used for the reduction of these dye compounds from industrial wastewater. But those approaches are time-consuming, costly, and pose disposal problems. Ultimately, adsorption onto AC is a well-established and cost-effective technique among the various treatment processes because of its simplicity in design, ease of operation, and high adsorption capacity (Vunain et al ., 2017). Therefore, it is extreme relevance to find suitable low-cost raw materials that are economically attractive and at the same time present similar or even better characteristics than the conventional ones. The use of waste materials for the preparation of AC is also very attractive from the point of view of their contribution to decrease the costs of waste disposal, therefore is used to help environmental protection. The

present study synthesized inexpensiveness adsorbent and in environmental friendly method for removal of toxic dye by using easily recyclable and environmentally friendly adsorbent.

1.3. Objective

1.3.1. General Objective

The general objective of this study was to synthesize and characterize AC-Fe_3O_4 nanocomposite and evaluate its MB dye removal performance from wastewater sample.

1.3.2. Specific Objectives

- To activate the *Jacaranda Mimosifolia* pod adsorbent material using thermal and chemical methods.
- To synthesize AC, Fe_3O_4 nanoparticles and AC-Fe_3O_4 nanocomposite.
- To characterize the synthesized activated carbon, Fe_3O_4 nanoparticles and AC-Fe_3O_4 nanocomposites using FTIR, TGA, XRD, and SEM.
- To evaluate performance of AC-Fe_3O_4 nanocomposite in removing MB dye from an aqueous solution.
- To determine the optimal adsorption parameters (temperature, pH, adsorbent dose, contact time, and initial MB concentration) for efficient removal of MB dye from an aqueous solution.
- To study the adsorption mechanism through adsorption isotherm and kinetic Models.

1.4. Significance of the Study

This study can be used to provide a method to remove non-biodegradable dye contaminant that pose serious health and environmental hazard using a simple, cost-effective, and environmentally friendly adsorption method.

The prepared composite adsorbent can be used for the removal of the MB dye from wastewater of different industries before the dye-contaminated wastewater is discharged into the environment. The research will assist in demonstrating insight on how to develop simple, cost effective, environmentally friendly, and easily available composite adsorbent that can be used to replace imported activated carbon or other commercially available expensive adsorbent materials. The conversion of JM biomass into a valuable AC supports the reduction of greenhouse gases, decrease the amounts of residuals accumulated in the environment and

reducing the environmental stress. Using the described by-products as adsorbents could be a good solution for huge quantities of these wastes in terms of sustainable development and green projects, as well as a means of cutting disposal costs.

The research will be essential for other researchers and academicians to perform additional investigation by expanding this examination. The costs of preparing activated carbon have historically been high. Using this bio -wastes as activated carbon precursors has substantial economic and environmental impact as converting undesirable agricultural waste to high-value adsorbents. Furthermore, using bio-waste residues as precursors for AC synthesis will reduce the importation of activated carbon from international markets. This study will provides important information about alternative and cheaper natural bio-adsorbents of cleaning contaminated water using locally available waste materials. This project will attempt to fill the gap in eco-friendly, recyclable and cost effective synthesis of activated carbon-magnetite composite for the removal of toxic dyes from industrial wastewater.

2. LITERATURE REVIEW

2.1. Wastewater

The world‘s water supplies have been contaminated due to large effluents containing toxic pollutants such as dyes, heavy metals, surfactants, personal care products, pesticides, and pharmaceuticals from agricultural, industrial, and municipal resources into water streams. Water contamination and its treatment have emerged out as an escalating challenge globally. Extraordinary efforts have been made to overcome the challenges of wastewater treatment in recent years (Rashid *et al.*, 2021). Wastewater is produced in different ways like in household, restaurant and industrial activities. The source of wastewater plays an important role on its properties and treated processes. Four categories of water are generally distinguished: (1) rainwater (runoff from impermeable surfaces), (2) domestic wastewater, (3) agricultural water and (4) industrial wastewaters (Crini et al., 2019). Domestic wastewater (house and restaurant wastewater) normally holds contaminants like vegetable materials, grease and scum detergents, and sediment (El-sayed et al ., 2020). Industrial wastewater may contain toxic chemicals and metals, organic wastes, radioactive elements, great quantities of sediment, high temperature waste or acidic/basic waste while storm wastewater may include; oil, fuel, insecticides, herbicides and residual sediments as shown in Figure1.

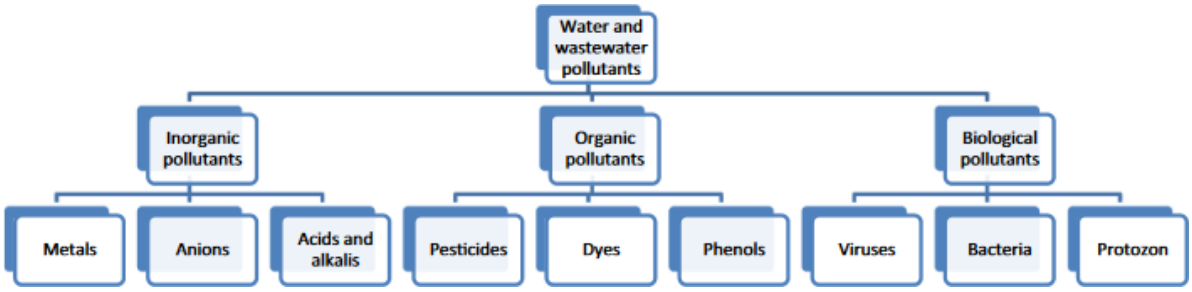

Figure 1: Types of Water and wastewater contaminants *(El-sayed et al ., 2020).*

In recent information, more than 100 thousand commercially dye products have discharged to the aquatic environment. Textile industries were the largest contributor to water pollution followed by paint, paper, leather, and printing industries (Santoso *et al*., 2020). Disposal of dye into environment is harmful to the aquatic life ecosystem, and posed negative impact to human health. Dye consisted of complex aromatic molecular structures, therefore very hard to

degrade. The consequences can be in the form of aesthetic disorders, such as discoloration and foul-smelling water and life disruption of water ecosystems due to reduction of sunlight penetration and depletion of oxygen level in water. The risk of dye pollution in water for human health includes the emergence of skin diseases upon contact with polluted water and digestive disorders from water consumption that m that may lead to the potential risk of cancer (Yagub *et al*., 2014).

2.1.1. Wastewater treatment methods

There are several treatment technologies employed to remove pollutants from water/wastewater includes flocculation, coagulation, biological oxidation, sedimentation, advanced oxidation processes (AOPs), oxidation with chemical oxidants (ozone or hydrogen peroxide, etc.), photo-catalytic oxidation/degradation, membrane processes, electrochemical oxidation/degradation, adsorption and combined methods (Adegoke et al., 2015, Jiang et al., 2011, Kurniawan et al., 2006). Different methods used in purification of water are given in Figure 2.

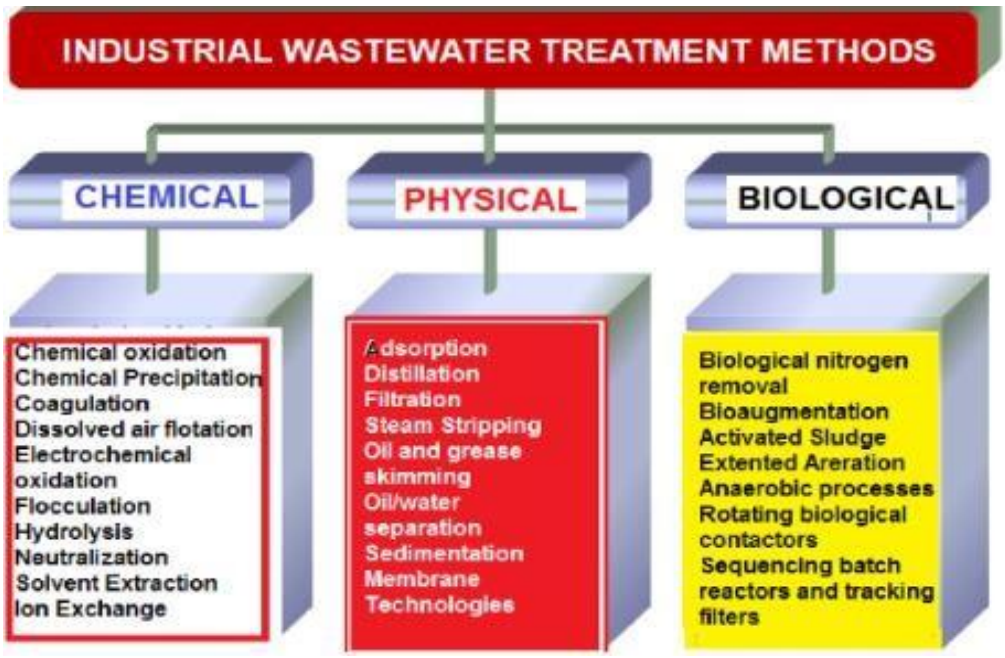

Figure 2:Different methods for purification of water (Singh et al., 2018).

Due to huge discharge in water, number of techniques for wastewater treatment has been developed (Adegoke et al., 2015, Quist-Jensen et al., 2015). However, most of these

technologies are not capable of fixing water pollutants in an effective way. Major threats and drawbacks to common water purification systems are given in Figure 3.

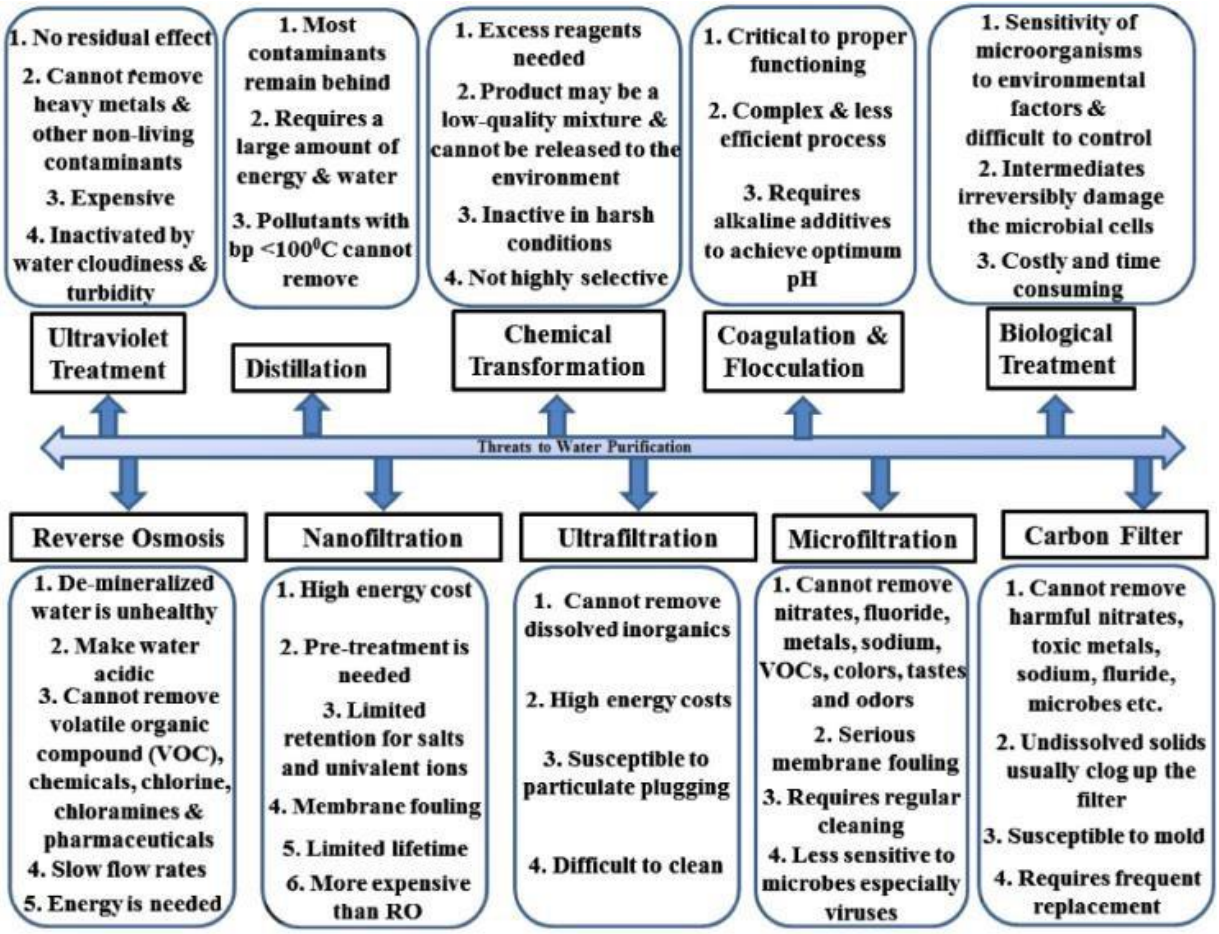

*Figure 3:*Some major treatment to conventional water purification systems (Singh et al., 2018).

2.2. Methylene blue dye

MB ($C_{16}H_{18}N_3SCl$) is a basic cationic dye with a molecular mass of 319.87 g/mol. The molecular structure and physical and chemical properties of MB is presented in Figure 4A and 4B. It is a cationic dye that gives a net positive charge when mixed with aqueous solutions due to the presence of chemical groups such as amine or sulfur. At room temperature, MB is solid, odorless, dark green powder and gives a blue solution if dissolved in water (Laysandra et al., 2017). It is used to several applications like the coating and coloring of paper, hair, cotton, and wool; it is also used as an indicator of oxidation-reduction and as a disinfectant, besides its many other medical usages in medicine, in pharmaceutical formulations, in

pesticide production, varnish, and lacquer manufacturing, among others (Zaghbani et al., 2007). Among different pollutant dye methylene blue (MB) is a model cationic dye employed by industries such textile industry for a variety of purposes such as in coloring paper, dyeing cotton, wools, silk, leather, and coating for paper stock (Aragaw *et al*., 2020).

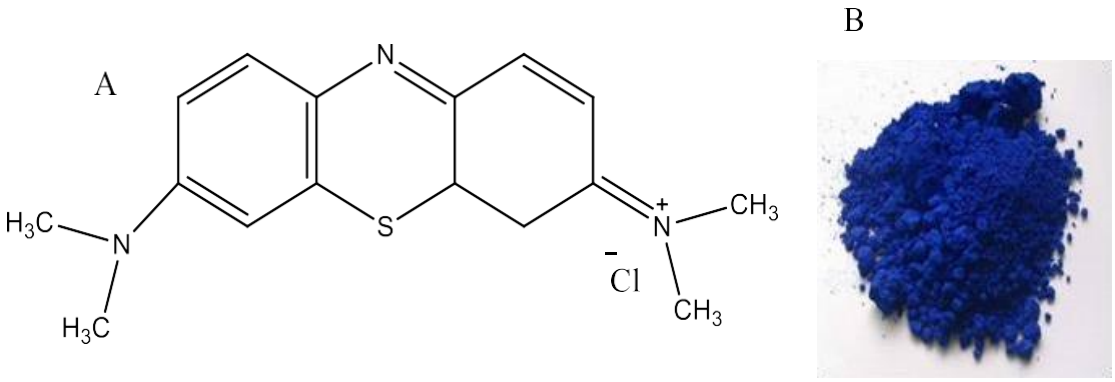

Figure 4:(A) Molecular structure of MB and (B) Powder of MB

2.2.1. Industrial and medicinal uses of methylene blue

MB is one of the most commonly utilized organic compounds. It is used to color paper, hair, cottons, and wools, as well as for biological staining. Cottons, wools, and silks were frequently dyed using this dye in the textile business (Miraboutalebi et al., 2017). In particular, methemoglobinemia and urinary tract infections are treated with MB injection. MB is also used to treat chronic urolithiasis, cutaneous viral infections, and manic-depressive psychosis, among other things. In a patient with septic shock, MB is also used to improve vascular tone and myocardial function. In general, MB is a safe medication that has a dose dependent hemolytic effect (Usall et al., 2016).

2.2.2. Methylene blue dye in industrial effluents

Textile, painting, rubber, leather, cosmetics, pharmaceuticals, food, paper, and plastics are just a few of the industries that produce dye effluents. The global textile industry is estimated to be worth around $1 trillion USD and its contribution towards total world exports is around 7%, employing 35 million people worldwide. The most prominent and destructive form of pollution, caused by the textile industry, is the water pollution due to the usage of dyes (Desore & Narula et al ., 2018). Textile effluents are both aesthetically polluted, and have

high salinity, chemical oxygen demand, and eco-toxicity, and due to their increasing ubiquity in surface water, can lead to adverse effects to human and wildlife health and to aquatic ecosystems in general. Of the different types of dyes, MB, which is commonly used in textile dyeing, paper printing, and other sectors, can eventually build up in industrial effluents and be discharged into receiving streams and other water sources (M. Mostafa et al ., 2015, Daud et al., 2017).

2.2.3. Adverse effects of methylene blue dye in the environment

Dye pollution is a hazard to ecological balance and human health because of its mutagenic, carcinogenic, and teratogenic effects when inhaled or absorbed via the skin. Massive and illegal releases of MB-contaminated wastewaters from textile mills into lakes and rivers have caused a severe threat to ecosystems, as the lack of dissolved oxygen in the water limits the growth of aquatic life (Guo et al., 2018). High concentrations of MB dye in aquatic environment stop the absorbing water's re-oxygenation potential and cut off sunlight, interrupting biological activity in aquatic life as well as the photosynthesis cycle of aquatic plants and algae (Zaghbani et al., 2007). MB is also directly hazardous to human health, as it is poisonous, mutagenic, and carcinogenic. Dyspnea, diarrhea, and tachycardia are just a few of the respiratory, digestive, and cardiovascular disorders it can induce (Sham & Notley, 2018). This dye can cause eye burns, which may be responsible for permanent injury to the eyes of human and animals. So, the treatment of wastewater contaminated by MB dye is the focus of considerable water treatment research (Khatri et al., 2015).

2.2.4. Adsorption of dyes

Despite the importance, uses of MB have harmful effects on humans and the environment because of its water solubility. It is noxious, a mutagenic reagent and is supposed to be a cancer-causing dye. Furthermore, MB is possibly harmful to human health and contributes to causing chronic toxicity(Kara *et al.*, 2021).In order to reduce the negative effects of dye contaminated wastewater on humans and the environment, the wastewater must be treated carefully before discharge into main streams. Adsorption is defined as the attachment or adherence of particles to the surface of a solid substance. It is a phase transfer process that is widely used in practice to remove substances from fluid phases (gases or liquids). Here, molecules or ions are removed from the aqueous solution by adsorption onto solid surfaces.

Solid surfaces are characterized by active, energy-rich sites that are able to interact with solutes in the adjacent aqueous phase due to their specific electronic and spatial properties (Worch et al., 2012). On the surface of the adsorbent material there are active adsorptive sites, which bind molecules (gas or liquid) from the adsorbate solution (Figure 5). Adsorption for the treatment of dyes from wastewater has recently sparked attention due to its cheap operating costs, ease of design, efficiency, and speed of dye removal. As shown in Figure 6, different adsorbent materials can be used for the removal of dye contaminants from wastewater (Singh et al., 2018).

Because of simplicity and cost effectiveness, adsorption technique is considered to be suitable for wastewater treatment. The adsorbent selection for removal of water contaminants depends on concentration and type of pollutant present in the water, efficiency and adsorption capacity for pollutant. Additionally the adsorbents should be non-toxic, cost effective, and easily available and can easily be regenerated. A large number of adsorbents such as natural materials, agricultural wastes and residues, industrial byproducts and biomass materials have been used for purification of water and wastewater (Bhatnagar et al., 2010).

Molecules can be adsorbed either physically or chemically. The mass transition, in which gaseous or liquid molecules are moved to a solid phase, might take the form of migration, diffusion, or convection (Figure 5) (Worch et al., 2012). Physisorption is defined by interactions such as Lewis acid-base, van der Waals, and Columbic; whereas chemisorption is distinguished by the formation of new adsorbate-adsorbent bonds (Yan et al., 2015, Monama et al., 2018).

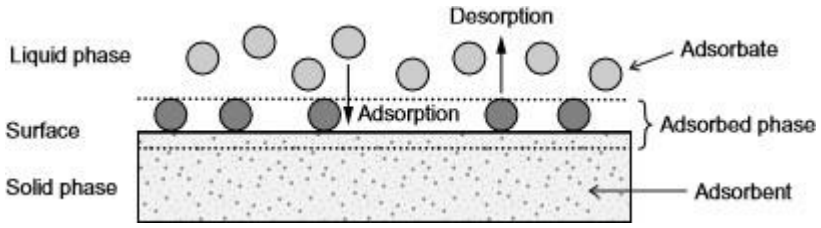

Figure 5:*Process of adsorption-desorption (Worch et al., 2012).*

Advances in science and technology have led to the evolution of several techniques for the removal of dyes from industrial (Ahmad *et al*., 2015). As sown in figure 2 a number of wastewater treatment technologies were investigated for the removal of MB dyes, such as adsorption, ion exchange, electrochemical, oxidation reduction, and biological method.

Among the dye removal technologies, adsorption appears the most economical method because of its inexpensiveness, easy working principle, and high pollutant uptake capacities or degradation but somehow adsorption may cause secondary disposal (Ahmad *et al.*, 2015; Yang *et al.*, 2016).

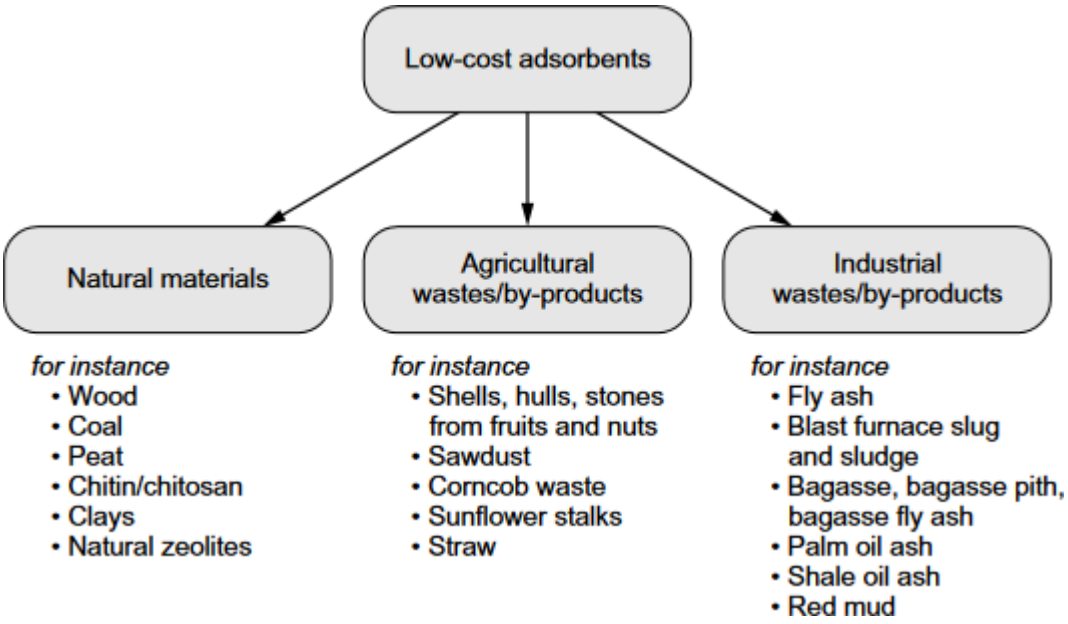

Figure 6: Low cost adsorbents (Singh et al., 2018).

2.2.5. Removal of Methylene Blue Using Adsorbent

Adsorption refers to a process in which atoms or molecules accumulate in a gas or liquid solution on the surface of a solid or liquid material and form a molecular or atomic thin layer. Adsorbent is the material on which the adsorption process is carried out and the adsorbate is the material that sits on the surface of the adsorbent (Rahimian et al., 2020). Despite the development of various technologies for dye waste water treatment, economic, effectiveness and rapid water treatment at a commercial level is still a challenging problem. previous research efforts have focused on the adsorption technology for the dye remediation from wastewater (Begum *et al.*, 2019). This technique can handle fairly large flow rates, producing a high quality effluent that does not result in the formation of harmful substances, such as ozone and free radicals. Moreover, it can remove or minimize different types of organic and inorganic pollutants and thus has a wider applicability in pollution control. Adsorption is hence recognized as the most versatile process used in lesser developing countries and is

currently being used extensively for the removal of organic pollutants from the aqueous media (Mohammed *et al*., 2014).

As shown in Figure 7 the contaminant or dye as absorber penetrates the adsorbent due to the potential for diffusion. The extent of infiltration potential is determined by the concentration of adsorbed material and the area available on the outer surface of the adsorbent. The adsorbed material penetrates the absorbent cavities after penetrating the outer surface of the adsorbent. All available areas are occupied during the chemical or physical adsorption process (Rahimian et al., 2020).

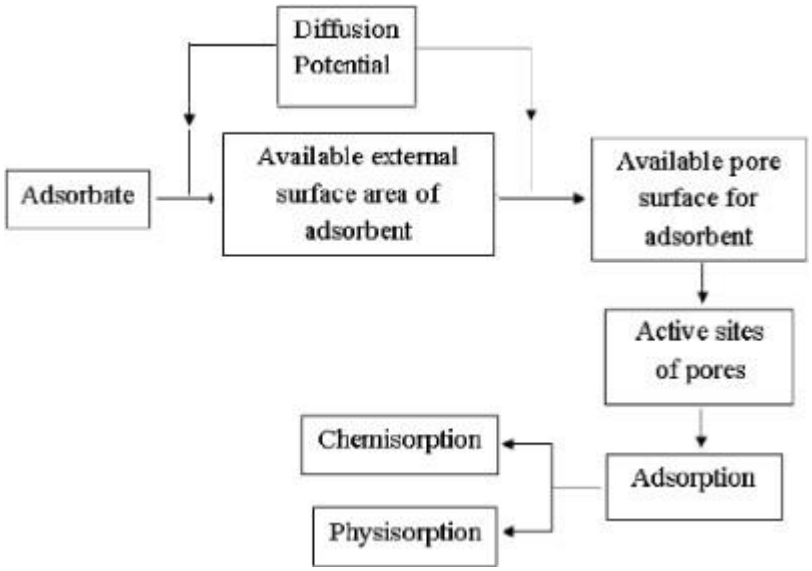

Figure 7: Pathways of adsorption process (Singh et al., 2018).

2.2.6. Agricultural wastes

Agricultural residues, fruits and vegetable peels are the discarded waste materials and find no application anywhere. They can be used as low cost adsorbent after little processing(Anastopoulos et al., 2014). Agricultural wastes are mainly composed of lignin and cellulose and act as attractive alternative adsorbents due to their specific structure and chemical properties. Specific functional groups such as alcohol, phenol, aldehyde, carboxyl and ketone are present in their polymer chains which help in the removal of various pollutants from water. A large number of agricultural wastes (Figure8) such as orange peel, pomelo peel, lemon peel, banana peel, rice husk, wheat bran, pulse seed coat, coconut shells, etc. have been

reported for purification of wastewater. Morphology and surface area of peels also play very important role during adsorption (Bhatnagar et al., 2015).

Figure *8*: Agricultural waste peels as low cost adsorbents (Singh et al., 2018).

2.3. Nanoparticles

Nanoparticles (NPs) are the products of nanotechnology usually ranging in size from 1 to 100 nm and have been classified on the basis of origin, dimensions, and structural configurations (Vikrant & Kim, 2018).These particles are transients between bulk materials and molecular structures with a high ratio of surface area to mass. Anthropogenic inorganic nanoparticles (metallic nanoparticles) possessing extremely small size and large surface to volume ratio have unique properties, such as magnetic and optical polarizability, electrical and thermal conductivity that have led to many applications with great scientific impetus as well as industrial significance. Noble metallic nanoparticles have significant utility in diverse fields, such as clinical diagnostics and therapeutics, electronics, cosmetics, textiles, food processing and packaging, wastewater treatment, environmental remediation and agriculture (Chaudhary et al., 2020).

Due to unique morphological (shape, size, and charge distribution) and physico-chemical properties of NPs, they find applications in almost every discipline of science, like space, energy, defense, communication, biomedicine, and agriculture. Use of NPs in disease diagnosis, imaging, treatment, drug delivery, tissue engineering, and cancer therapeutics is also increasing tremendously (Macys, 2005). However, application of NPs in biological

entities, especially humans, is very critical, and the NPs used in biomedical applications should preferably be from green sources. Taking into consideration various factors, such as biocompatibility, bioavailability, bio-distribution, and most importantly biosafety of NPs, the current trend of synthesis of NPs is moving towards the safer side. NPs are mostly synthesized by physical and chemical methods such laser ablation, mechanical milling, electro explosion, and sol-gel, but they are hazardous for environmental and human health (Cheng et al., 2016). The trend to synthesize NPs from alternative, environmentally safe, cost-effective, and non-toxic green methods is increasing.

2.3.1. Metal Oxide nanoparticles

Nano metal oxides (NMOs) show an effective and specific adsorption towards various aquatic pollutants. However, they are usually present as fine or ultrafine particles, which often lead to problems such as activity loss due to agglomeration, difficult separation, and excessive pressure drops when applied in flow-through systems (Fu et al., 2018). An effective approach to overcome this technical obstacle is to fabricate hybrid adsorbents by coating NMOs particles into/onto porous supports of larger size. The transition-metal oxides (TMOs), which have attracted the attention of materials scientists and engineers, constitute a fascinating class of inorganic solids (T. Ahmad et al., 2021). Their magnetic, electrical, optical, catalytic and mechanical properties make them technologically useful. TMOs are compounds composed of oxygen atoms bound to transition metals, and are commonly utilized in several electronic applications due to their superior semiconducting properties (Vazinishayan et al., 2018). TMOs show remarkable physical properties among which spinal oxides (particularly ferrites) show comparably good and interesting magnetic and electrical properties, which make the ferrites particularly very attractive for several novel applications.

In the recent years, the Transition Metal Oxide Nanoparticles (TMO NPs) have emerged as potential candidates for a number of scientific applications including Biomedical Applications, Photovoltaic Applications Resistive Switching Applications and many more. Besides physical routes of synthesis of nanoparticles, the chemical routes are preferred because of the availability many easy synthesis techniques such as Hydrothermal and Sol-Gel etc. Further, large scale production and cost-effective synthesis of nanomaterials is possible

through chemical synthesis to match industry (Adiba et al., 2019). MO adsorbents applied for wastewaters treatment have included iron oxide (Fe_3O_4), zinc oxide (ZnO), titanium dioxide (TiO_2), magnesium oxide (MgO), alumina oxide (Al_2O_3), and zirconium oxide (ZrO_2). Amongst them, iron oxide nanoparticles (IONs) have garnered increasing attention due to the attractive properties such as high specific surface area, strong adsorption affinities toward organic pollutants, and more importantly the magnetism property (Lima et al., 2021).

2.3.2. Magnetite (Fe_3O_4) Nanoparticles

Despite the development of various technologies for dye waste water treatment, economic, effectiveness and rapid water treatment at a commercial level is still a challenging problem. Previous research efforts have focused on the adsorption technology for the dye remediation from wastewater (Begum *et al.*, 2019). This technique can handle fairly large flow rates, producing a high quality effluent that does not result in the formation of harmful substances, such as ozone and free radicals. Moreover, it can remove or minimize different types of organic and inorganic pollutants and thus has a wider applicability in pollution control. Adsorption is hence recognized as the most versatile process used in lesser developing countries and is currently being used extensively for the removal of organic pollutants from the aqueous media (Mohammed *et al*., 2014).

Fe_3O_4 is derived from various sources such as black iron oxide, magnetic iron ore, loadstone, ferrous ferrite and Hercules stone. Fe_3O_4 has face centered cubic spinel structure with both divalent and trivalent iron in it. All of the Fe^{2+} ions reside in half of the octahedral sites whereas the Fe^{3+} ions are divided evenly across the remaining the remaining available octahedral and the tetrahedral sites (Mohapatra et al., 2011). Magnetite has been attracting growing interest as they exhibit unique electrical, optical and magnetic properties for numerous applications such as production of inorganic pigments, magnetic storage media, development of gas sensors as well as electronic and optical devices, information storage, color imaging, magneto caloric refrigeration, bioprocessing, and wastewater treatment adsorbents (Lin et al., 2021). The most assuring and interesting candidate is known to be Fe_3O_4 NPs because of its wide range of properties including active surface for adsorption of ligands and metals for recyclable catalysts. They are also known for their magnificent electronic and magnetic properties due to charge transfer between Fe^{3+} and Fe^{2+} ions. Thus,

they can be used to synthesize magnetically recyclable catalyst which can easily degrade the organic dyes reducing their hazardous effects. Many researchers have synthesized Fe_3O_4 NPs and used in various degradation studies (Mohapatra et al., 2011). Magnetic Nanoparticles (MNPs) are preferred over other metal catalysts for their non-toxic, ubiquitous and cost effectiveness. They have indeed become increasingly appealing in the field of catalysis over the last decade as they combine their fascinatingly reactive properties with an easy environmental benign mode of recovery (Lin et al., 2021). The separation of MNPs indulges them in the prominent industrial applications. It could be used bare or by plating it with an appropriate metal that is catalytically active MNPs synthesized in situ between the reaction of hydrazine monohydrate and iron salt in methanol at high temperature have proved to be effective catalysts in specifically reducing aromatic nitro groups into anilines with the aid of a reducing agent like hydrazine. MNPs have also involved in methylene blue degradation accomplished by sodium borohydride that have an escalated rate of degradation reaction after the addition of MNPs (L. Zhang et al., 2012).

A lot of efforts have been taken to understand the mechanism of NPs formation in solutions via nucleation and growth (Thanh et al., 2014). Physical methods include metal evaporation by sputtering, ball milling and electrode deposition. These methods are advantageous since they allow mass production and high-purity nanomaterials but they do not offer a good control on the size and shape of the nanoparticle. Solution phase chemical methods offer effective ways to produce MNPs because of their precise control over the composition, size and structure of the resultant materials. These chemical methods include co-precipitation, gas-phase deposition, sol–gel method, oxidation method, flow injection, microbial, herbal plants extract, thermal decomposition or reduction, hydrothermal synthesis, laser pyrolysis techniques and herbal extract mediated biosynthesis There are a lot of successful studies where Fe_3O_4-NPs can be synthesized using different biological routes, however plant extract is the most extensively used in green synthesis because it can be obtained easily, large-scale production, cost effective and environmental benign (Ajinkya et al., 2020). In addition, extracts from plants can act as reducing and stabilizing agents in the nanoparticles synthesis which might be due to the presence of phytochemicals. Phytochemicals are compounds that are produced by plant itself. Furthermore, the applications of Fe_3O_4 -NPs might depend on the substrate used as well. Rice straw, fruit peels and coffee waste hydro char are natural waste

which we might think they are worthless. But, the Fe_3O_4-NPs synthesized by waste can be useful too. Based on studies, Fe_3O_4-NPs prepared by tea residue, coffee waste hydro char and corn can be used in arsenic removal (Lunge et al., 2014), Acid Red 17 (azo dye) removal and drug delivery applications (Patra et al., 2017) respectively.

2.4. Nanocomposites

Nanocomposites are composites in which at least one of the phases demonstrates dimensions in the nanometer range. Nanocomposites suggest rare properties that ascend from their small size, large surface area, and the relations of phases at their interfaces. They are striking for their prospective to develop performance of drugs, catalysts, biomaterials and other high value added materials. Nanocomposites offer an exceptionally extensive range of prospective applications from electronics, optical communications and biological systems to new materials. Currently, nanocomposites offer new technology and business opportunities for all zones of industry, in addition to being environmentally friendly (Din et al.,2019). From many previous findings, nanomaterials have been produced as a novel high efficiency adsorbent for heavy metal removal from wastewater (Hua et al., 2012; Ray & Shipley, 2015; Wang, 2012; Yang et al., 2019). The development of well- designed nanoadsorbents from metal oxides and carbon sources have been utilized in broad industrial applications including bioprocess, environmental remediation and their unique characteristics such as high reactivity, biocompatibility, high surface to volume ratio, reversibility, metal binding capability and comparatively low cost as well as high degree of functionalization make them as potential high efficient adsorbents for wastewater treatment and water purification applications (Mohd et al., 2017; Dave & Chopda et al., 2014; Qu et al.,2013) also reported the capability of nanoadsorbents that can adsorb the contaminants in terms of molecular size, hydrophobicity and speciation behaviour. Besides that, nanoadsorbents are also enabling the manufacturing processes to consume raw materials efficiently without releasing any toxic by-products (Burakov et al., 2018).

Nanocomposites consist of a matrix in which fillers are incorporated based on the properties to be improved. The matrix and the reinforcing fillers may be organic or inorganic. Based on the matrices used, nanocomposites may be classified as polymer matrix nanocomposites, ceramic matrix nanocomposites, or metal matrix nanocomposites. Nanocomposites are

synthesized with multi-phase solid materials, which are a combination of two or more components including a continuous and discontinuous phase with at least one within the nano-scaled dimension (Ravichandran et al., 2018).

2.5. Types of Adsorbents

Different types of adsorbents are classified into natural adsorbents and synthetic adsorbents. Natural adsorbents include charcoal, clays, clay minerals, zeolites, and ores. These natural materials, in many instances are relatively cheap, abundant in supply and have significant potential for modification and ultimately enhancement of their adsorption capabilities (Rashid *et al*., 2021). Synthetic adsorbents are adsorbents prepared from Agricultural products and wastes, house hold wastes, Industrial wastes, sewage sludge and polymeric adsorbents. Each adsorbent has its own characteristics such as porosity, pore structure and nature of its adsorbing surfaces. Many waste materials used include fruit wastes, coconut shell, scrap tires, bark and other tannin-rich materials, sawdust, rice husk, petroleum wastes, fertilizer wastes, fly ash, sugar industry wastes blast furnace slag, chitosan and seafood processing wastes, seaweed and algae, peat moss, clays, red mud, zeolites, sediment and soil, ore minerals (Kandisa *et al*., 2016).

2.5.1. Activated Carbon as Adsorbent

In the adsorption process, adsorbent primarily depends on the surface chemistry and pore structure of the material. Method of activation and nature of precursor tremendously affect the surface functional groups and pore structure. The surface functional groups provide vital information involving removal of cationic and anionic adsorbate (Musa et al., 2018). For example, when activated carbon is treated with acid, the activated carbon will have negatively charged acid groups and able to absorb cationic adsorbate and vice versa et al., 2010). Activated carbon (AC) has been the most promising adsorbent. It has high adsorption efficiency, large surface area, high porosity structure, and high surface reactivity (Moosavi et al., 2020). Different kinds of AC are available and used as catalyst or support of a catalyst and adsorbents. Therefore, for industrial scale application, AC is one of the most important adsorbent materials. Activated carbon can be made from biomass as well as other carbonaceous materials such as fossil, waste, or renewable sources which activated using

chemical activation (such as acid, base, or salt activation) or physical activation (steam/ air/gas). Activated carbons obtained from these precursors may show physical, chemical and adsorption properties that may vary significantly with respect to those properties of adsorbents obtained from conventional raw materials. Actually, lignocellulosic residues from crops and fruit production can be considered as the most appropriate precursors for a cost-effective preparation of activated carbons based on the fact that several billion tons of these wastes are available worldwide (Trevi˜no *et al*, 2013). Activated carbon is used to purify liquids and gases in a variety of applications, including municipal drinking water, food and beverage processing, odor removal, industrial pollution control. Activated carbon is produced from carbonaceous source materials, such as coconuts, nutshells, coal, peat and wood. The primary raw material used for activated carbon is any organic material with high carbon content. Adsorption is a process where a solid is used for removing a soluble substance from the water. In this process active carbon is the solid. Activated carbon is produced specifically so as to achieve a very big internal surface (between 500 - 1500 m^2/g) (Vunain et al., 2017). This big internal surface makes active carbon ideal for adsorption. AC has difficulties in separation from water bodies and generates secondary pollution. Meanwhile, non-recyclability is cost-ineffective and may limit its applications on a large scale in many fields. Traditional methods, such as filtration, can cause the blockage of filters or the loss of C (Serrano et al., 2014).Thus, a material that would overcome these limitations should be developed. Different solutions have been studied. Depending on the characteristics of industrial wastewater, magnetic separation can be a promising treatment technique with easy and fast recovery. The use of magnetic adsorbents can enhance the thermal stability and the cross-linking density of the adsorbents. This technique has the potential to improve times and efficiencies of urban and drinking water treatment plants. This technique might also substitute industrial wastewater treatments. This technique combines a physicochemical phase of adsorption and a magnetic phase of filtration. The adsorbents combated of AC with magnetic particles possess high adsorption capacity and easily recover through the magnet. Many studies on the combination of AC and magnetic particles have been conducted (Moosavi et al., 2020).

2.5.2. *Jacaranda Mimosifolia*

Jacaranda Mimosifolia (D. Don) is an ornamental tree belonging to the family *Bignoniaceae*, widely distributed in tropical and subtropical areas of the world. The forest species, *Jacaranda mimosifolia* is a plant easily found in most countries and its dense flowering and purple color are used in the ornamentation of squares and parks. Its fruits are dense, rounded, and woody in the form of capsules. Extracts of various organs of *J. mimosifolia* are used in several countries including Bangladesh, India and Pakistan to treat hypertension, ulcers, wounds, diarrhea, dysentery and amoebic infections (Naz *et al.*, 2020). *Jacaranda mimosifolia* (shown in Figure 9) is a plant easily found also found in Ethiopia; its fruits are dense, rounded, and woody in the form of capsules. They are produced in large volumes, and when ripen, open, releasing the seeds (Georgin *et al.*, 2021). Jacaranda has been traditionally used in treating skin disorders, venereal diseases, leishmaniasis, colds and rheumatism (Mohd Udaiyappan *et al*., 2017). In Ethiopia fruit *Jacaranda mimosifolia* is a waste found on the ground around the Jacaranda tree.

(a) (b)

Figure 7: Image (a) Jacaranda plant and (b) fruit (seed pod) of *Jacaranda mimosifolia.*

2.6. Activation of Activated Carbon

The precursor composition may have a significant effect on the micropore structure of the end product and, as a consequence, in the final adsorption properties of activated carbons (Vunain et al., 2017). Generally, two types of activation processes are involved in the production of activated carbons by way of physical activation and chemical activation.

2.6.1. Physical activation

Physical activation (sometimes also called thermal activation) is the process of slow oxidation of the char with mild oxidizing agents such as steam and carbon dioxide at temperatures usually between 400^0C and 1000^0C (Moosavi et al., 2020). In this process, the disorganized material is removed first with the subsequent increase in pore volume and by this the elementary crystallites become exposed to the action of the activating agent for further development of porosity with increasing burn-off. The slow oxidation process creates new porosity or enlarges the existing pores. Carbon dioxide is usually preferred over steam because of its low reactivity that permits controlling oxidation rates such that uniform porosity is developed (Contescu et al., 2018).

The process of physical activation comprises two steps: (a) Carbonization is the first stage and involves the formation of a char, which is normally nonporous, by pyrolysis of the precursor at temperatures in the range between 400 and 850 °C, and sometimes reaches 1000 °C, in an inert, usually nitrogen atmosphere and in the presence of physical agents like heat, gases (carbon dioxide, helium and nitrogen) and steam to disrupt the cross-linkages present between C atoms; (b) Activation is the second stage and involves contacting the char with an oxidizing gas, such as carbon dioxide, steam, air or their mixtures, in the temperature range between 600 and 900 °C, which results in the removal of the more disorganized carbon and the formation of a well-developed micropore structure. The activation gas is usually CO_2, since it is clean, easy to handle and it facilitates control of the activation process because of the slow reaction rate at temperatures around 800 °C. Such a relatively high pyrolysis temperature further enhance the porosity of the biochar (Adegoke et al., 2015, Rodríguez et al., 2012). Various activating agents are reported in the literature, which includes carbon dioxide, air, nitrogen, steam, oxygen etc (S. Wang et al., 2017). In general, the mild oxidizing agents like, steam and carbon dioxide are commonly used for the thermal activation of biochar, because they favor slow oxidation process, leading to the formation of new pores and enlargement of the existing pores (Contescu et al., 2018). The activating agent has a significant effect on the C properties and the degree of activation. Liu reported the production of super activated carbon (using KOH) with the maximum surface area value of 3362 m^2/g and concluded that activation temperature (800 °C), time, and impregnation ratio had the highest effects on

improving the surface area. The alkali KOH is a highly attractive activating agent (Moosavi et al., 2020).

Physical activation method is relatively economically feasible, cheap and eco-friendly than the chemical based activation method. The chief parameters which affect the quality and characteristic properties of biochar are activation time, temperature and flow rate of gas during physical activation method (Liou et al., 2010). The most important variables in the gasification process from the point of view of porosity development are the activating agent, the final bum-off reached, and the presence of inorganic impurities that catalyze or inhibit the gasification reaction. It has been reported that surface area and porosity of biochar increases with increase in the flow rate of gas and process temperature whereas the activation time possesses negative effect after a certain time interval (Devi et al., 2017, Moosavi et al., 2020).

2.6.2. Chemical activation

Chemical activation is based on char impregnation with chemicals ($ZnCl_2$, KOH, and H_3PO_4) which promote dehydration, polycondensation, and gasification reactions at lower temperatures than those needed for physical activation. The yield is higher, but the process requires extensive washing of final product for elimination of chemicals, which is perceived as an environmental penalty (Contescu et al., 2018, Zhong *et al*., 2012). Chemical activation produces activated carbons with higher surface area and a higher yield at a lower temperature than physical activation (Rashed et al., 2013). Recent research studies showed that the phosphoric acid activation using microwave as a heating method yielded activated carbons with a better quality at a lower temperature than the normal heating method, which results a great energy saving (Demirbas et al., 2009). In particular, the chemical activation appears to be the most used procedure for the preparation of adsorbents for water purification (Liu et al., 2010). The chemical activation process is preferred over the physical activation process to make coal-based activated carbon. Compared with physical activation, chemical activation will lower the inherent mineral content of the coal and produce activated carbon with a significantly low ash content. Another evident advantage of the chemical activation method is that the AC yields are generally extremely high in the presence of chemicals. It is carried out in a single step, performed at lower temperatures and, therefore, resulting in the development

of a better porous structure (Adegoke et al., 2015). The surface area of the activated carbon via chemical activation is also generally high. Another study also proposed that chemical activation can cut energy consumption compared with the physical activation process because the activating agent is not required to be heated, and pyrolysis and activation are combined into one stage. However, physical activation is used for commercialized activated carbon thus far because of its low production cost (Moosavi et al., 2020).

In the chemical activation process, carbonization and activation are carried out simultaneously, with the precursor being mixed with chemical activating agents, such as dehydrating agents and oxidants. Activation of carbon is used to enlarge the diameter of the fine pores, create new pores and can serve as ideal support media for iron impregnation. The selection of the precursor for the preparation of activated carbon depends upon availability, cost, carbon content, and ease of activation (Adegoke et al., 2015, Rajbhandari et al., 2010).

2.7. Characterization of Nanoparticles and Composite

The characterization of nanomaterials is important for understanding their properties and applications. Strategies used for their fabrication and characterization are going to be improved day by day. Control over size and shape of nanoparticles is very important for their potential applications in various fields (Begum et al., 2018). The common methods used for the characterization of nanoparticles include, Ultraviolet visible (UV–Vis) spectroscopy, Scanning electron microscopy (SEM), Transmission electron microscopy (TEM), low energy electron diffraction (LEED), Extended X-ray absorption fine structure (EXAFS) used for the detection of surface topography, and Secondary ion mass spectroscopy (SIMS), Auger electron spectra (AES), Electron probe microanalysis (EPMA) (Mourdikoudis et al., 2018). Each technique has its own advantages and disadvantages and it is hard to compare one technique to another because each technique has a specific purpose and used to get a specific information that cannot be obtained from the other one (K. Zhang et al., 2015).

2.7.1. Fourier transform infrared spectroscopy

Fourier Transform Infrared, the preferred method of infrared (IR) spectroscopy. In IR spectroscopy, IR radiation is passed through a sample. Some of the IR radiation is absorbed

by the sample and some of it is passed through (transmitted). The resulting spectrum represents the molecular absorption and transmission, creating a molecular fingerprint of the sample. As two finger prints never match, similarly no two unique molecular structures produce the same IR spectrum (Yao et al., 2015). The functional groups of the materials were determined by using FTIR spectrometer. The infrared spectra is a fingerprint for identification by the comparison of the spectra from an _'unknown'' with previously recorded reference spectra. The vibrational spectra of a molecule are considered to be an important physical property. It is a unique characteristic of the molecule. In the absence of a suitable reference database, it is possible to effect a basic interpretation of the spectrum from first principles, leading to characterization, and possibly even identification of an unknown sample (Coates et al., 2006). However, the application of FTIR in the characterization of functionalized nanoparticles could be difficult because it may not reveal the chemical bonds between the nanoparticles and the functional molecules based on a database of known vibration frequencies. This is because the chemical bond between the functionalized molecules and the nano-material is usually novel, and thus, a strategy must be developed in order to provide evidence about the resonant vibration information between the grafted molecules and the nano-sized particles (Baudot et al., 2010). Biomolecules those are responsible for capping, reduction and stabilizer, are identified by using FT-IR (Ijaz et al., 2020).

2.7.2. X -ray diffraction

XRD is used for the determination of crystal structure, calculation of crystalline nanoparticles size and for confirmation of nanoparticles (Ijaz et al., 2020). The crystalline structure of nanoparticles can be calculated by using Debye Scherrer s equation (Muniz et al., 2016). The approximate average crystallite size of nanoparticles was determined by applying the Scherer formula:

$$D = \frac{0.9\lambda}{\beta\cos\theta} \quad (1)$$

Where D is the average particle size, λ wave length of the Cu-Kα irradiation, β the full width at half maximum intensity of the diffraction peak and θ is the diffraction angle. It provides information on structures, phases, preferred crystal orientations (texture), and other structural parameters, such as average grain size, crystallinity, strain, and crystal defects. XRD peaks

are produced by constructive interference of a monochromatic beam of X-rays scattered at specific angles from each set of lattice planes in a sample. The peak intensities are determined by the atomic positions within the lattice planes. An online search of a standard database for X-ray powder diffraction patterns enables quick phase identification for a large variety of crystalline samples (Thurston et al., 2017).

2.7.3. Scanning electron microscope (SEM)

SEM gives high resolution images of the surface of a sample. Image formed by using electron beams of SEM used to characterized shape, size, morphology and distribution of synthesized nanoparticles (Ijaz et al., 2020). The scanning electron microscope works as same principle as an optical microscope, but it measures the electrons scattered from the sample rather than photon. Because electrons can be accelerated by an electric potential, the wavelength can be made shorter than the one of photons. This makes the SEM capable of magnifying images up to 200,000 times and measures the particle size and characterization, Conductive or sputter coated sample involved and the sensitivity down to 1nm (Kaur & Kaur et al., 2019).

2.7.4. Thermal gravimetric analysis (TGA)

Thermogravimetric analysis or thermal gravimetric analysis (TGA) is a method of thermal analysis in which the mass of a sample is measured over time as the temperature changes. This measurement provides information about physical phenomena, such as phase transitions, absorption, adsorption and desorption; as well as chemical phenomena including chemisorption, thermal decomposition, and solid-gas reactions (e.g., oxidation or reduction) (Mani et al., 2010). Thermogravimetric analysis is conducted on an instrument referred to as a Thermogravimetric analyzer. A Thermogravimetric analyzer continuously measures mass while the temperature of a sample is changed over time. Mass, temperature, and time are considered base measurements in thermogravimetric analysis while many additional measures may be derived from these three base measurements. Thermogravimetric analysis is a widely used technique to obtain precise weight loss profile during thermal decomposition (Saadatkhah et al., 2020, Kumar et al., 2009).

2.8. Kinetics of Adsorption

Adsorption is one of the most widely applied techniques for pollutant removal from contaminated media. When adsorption is concerned, thermodynamic and kinetic aspects should be involved to know more details about its performance and mechanisms.

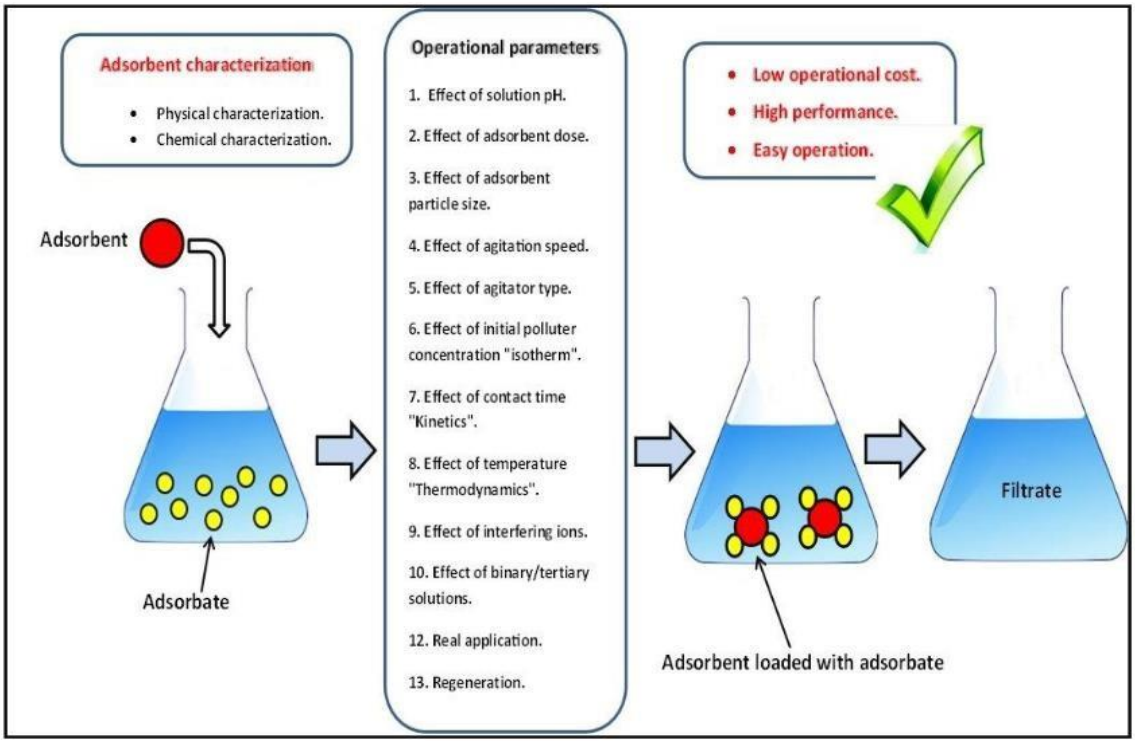

Figure 8: Schematic diagram of batch adsorption (Elwakeel et al., 2020).

Kinetic performance of a given adsorbent provides great significance for the pilot application. Adsorption kinetics is the measure of the adsorption uptake with respect to time at a constant pressure or concentration and is employed to measure the diffusion of adsorbate in the pores. From the kinetic analysis, the solute uptake rate, which determines the residence time required for completion of adsorption reaction, may be established. Also, one can know the scale of an adsorption apparatus based on the kinetic information (H. Qiu et al., 2009). Kinetics study helps to select optimum operating conditions for the full-scale batch process, which have been applicable to investigate the mechanism of adsorption and potential rate-controlling steps. Kinetic parameters are significant for the prediction of adsorption rate, and give useful information for designing and modeling the adsorption processes (Batool et al., 2018). Several kinetic models such as the pseudo first- and second-order equations, intra-

particle diffusion and Elovich equations are used to interpret the time dependent experimental data and examine the controlling mechanism of adsorption process (Rodrigues et al., 2009, Chen et al., 2007).

2.8.1. Pseudo-first-order model

The first-order model is believed to be the earliest model and it was developed by Lagragren in 1898 (H. Qiu et al., 2009). To describe the kinetic process of liquid-solid phase adsorption, it is generally used in the form proposed by Ho and McKay as:-

$$Lo(qe - qt) = -\frac{K_1}{2.303}t + Logqe \quad (2)$$

Where q_e and q_t (mg/g) are the adsorption capacities at equilibrium and at a time t (min), respectively, K_1 (min^{-1}) is the pseudo first order rate constant for the kinetic model (Y. Wang et al., 2021).

2.8.2. Pseudo-second-order model

It was not very popular until 1999 when Ho and McKay analyzed a number of experimental results taken from the literature, and arrived at the conclusion that, ―for all of the systems studied, the pseudo-second order reaction kinetics provide the best correlation of the experimental data‖ (Simonin et al., 2016). Currently, the pseudo-second-order rate equation, popularized by Ho and McKay, is probably the most widely used model for adsorption kinetics. Most of the time this equation is used when the first-order model fails and the equation for this model is written as:-

$$\frac{t}{qt} = \frac{1}{K_2 qe^2} + \frac{1}{qe}t \quad (3)$$

where q_e(mg/g) is the adsorption capacities at equilibrium; K_2(g/(mg min)) is the equilibrium rate constant of pseudo-second order adsorption (W. Y. Huang et al., 2014;S. J. Liu et al., 2016;Song et al., 2020).

2.9. Adsorption Isotherm Models

Adsorption isotherms have been of great importance to research dealing with environmental protection and adsorption techniques. An adsorption isotherm is a graph that represents the variation in the amount of adsorbate adsorbed on the surface of the adsorbent with the change

in pressure at a constant temperature. The adsorption isotherm experiments were used to determine the maximum phosphate adsorption capacities of the adsorbent. It the most suitable way to evaluate the adsorption process as well as to understand the interrelation between the amounts of adsorbate on the adsorbent surface to its concentration (Ayawei et al., 2017). The adsorption isotherm models are used to describe the phenomenon governing the retention or release of a substance from the aqueous porous media or aquatic environments to a solid phase at a constant temperature and pH. Among numerous isotherm models, Langmuir and Freundlich isotherm models are most widely used models to describe the single-solute adsorption because of the corresponding simple mathematical forms and excellent fitting performance (Hu & Zhang et al., 2019).

In this study, Langmuir and Freundlich models were used to fit the isotherms data for the adsorption of MB at pH = 7 and room temperature for assessing the adsorption behavior of the adsorbents.

2.9.1. Langmuir adsorption isotherm model

The Langmuir adsorption isotherm is used to describe the equilibrium between adsorbate and adsorbent system, where the adsorbate adsorption is limited to one molecular layer at or before a relative pressure of unity is reached. The isotherm initially proposed by Langmuir in 1918 is generally suitable for describing the chemisorption process when ionic or covalent chemical bonds are formed between the adsorbent and the adsorbate. The Langmuir adsorption isotherm describes the surface as homogeneous, assuming that there is no lateral interaction between adjacent adsorbed molecules when a single molecule occupies a single surface site. Langmuir adsorption isotherms are based on the assumption that the reactive groups are homogeneously distributed over the particulate's surface and that there is no lateral interaction. Langmuir pictured monolayer formation to occur on the basis of a specific binding interaction between adsorbate molecules and distinct solid surface sites. This picture was originally founded on the results of experiments performed with hydrogen and other small molecules in the presence of heated metal filaments at very low pressures. In Langmuir 1918, this model was already broadly generalized to include cases where monolayer or multilayer formation occurs as well as cases ranging from highly regular surfaces to completely amorphous surfaces containing an abundance of different adsorption sites. The

Langmuir theory of adsorption is useful for modeling and designing engineering processes, both qualitatively and quantitatively (Swenson & Stadie et al., 2019).The Langmuir model assumes that there is no interaction between the adsorbate molecules and the adsorption is localized in a monolayer form (Limousin et al., 2007). The Langmuir adsorption isotherm shows the equilibrium distribution of the ions between the solid and liquid phases. This model has been successfully applied to many real adsorption processes (Bilgiç & Çimen et al., 2019).The equation for Langmuir adsorption isotherm can be described as:-

$$\frac{C_e}{q_e} = \frac{1}{q_m} ce + \frac{1}{q_{mK_L}} \quad (4)$$

$$R_L = \frac{1}{1+K_L C_0} \quad (5)$$

Where, Ce = the equilibrium concentration of phosphate in the solution (mg/L), qe = the amount of phosphate adsorbed per gram of the adsorbent at equilibrium (mg/g), q_m = maximum monolayer coverage capacity (mg/g) or the maximum uptake corresponding to the site saturation, and K_L = Langmuir isotherm constant (L/mg) representing the ratio of adsorption and desorption rates. The separation factor R_L in eq (4) was used to evaluate the nature of the Langmuir isotherm. The R_L value tells the type of isotherm to be unfavorable ($R_L > 1$), linear ($R_L=1$), irreversible($R_L=0$), $0<R_L<1$ means that the reaction is well reversible, and favorable ($R_L<1$) (Y. Zhang et al., 2020; Y. Wang et al., 2021; Ajmal et al., 2018).

2.9.2. Freundlich adsorption isotherm model

The Freundlich isotherm model is an empirical relationship describing the adsorption of solutes from a liquid to a solid surface and assumes that different sites with several adsorption energies are involved. Freundlich isotherm model is the most important multi-site adsorption isotherm for heterogeneous surfaces (Deliyanni et al., 2007). It is one of the oldest models which are extensively used; it was developed by Freundlich in 1932**.** The Freundlich adsorption isotherm model is an empirical model expressed by the equation:

$$Log_e = \frac{1}{n} LogC_e + LogK_F \quad (6)$$

Where qe is the amount of phosphate adsorbed per gram of the adsorbent at equilibrium (mg/g), Ce is the equilibrium concentration of phosphate in the solution (mg/L), KF is the Freundlich constant denoting adsorption capacity of the adsorbent (mg/g) or the distribution

coefficient that represents the quantity of adsorbate adsorbed onto adsorbent for unit equilibrium concentration, *n* is the heterogeneity factor which is related to the intensity of adsorption (mg/L), and 1/*n* is an empirical constant related to the magnitude of the adsorption or surface heterogeneity. It also indicates the relative distribution of the energy and the heterogeneity of the adsorbate sites (Ayawei et al., 2017). A linear plot of Logqe versus LogCe provides the *K*F and *n* values. The Freundlich isotherm model is responsible for the heterogeneity of the adsorbent sites. For this study, Langmuir and Freundlich adsorption isotherm models were employed to describe the experimental results of phosphate ions adsorption.

2.10. Parameters that affects dye adsorption process

2.10.1. Solution pH

One of the most critical parameter determining adsorption process has been identified as the pH of the aqueous solution. It affects dye chemistry in the solution as well as the degree of ionization of the solute, the surface charge of the adsorbent, and dissociation of functional groups on the active sites of the adsorbent. Protonation of the dye occurs at a low pH, resulting in reduced dye adsorption in acidic media. At low pH, dye removal is inhibited, owing to greater competition between protons and dye molecules for the same binding sites. The dye gets more deprotonated as the pH of the solution rises, increasing the negative charge density on the adsorbent's surface. As a result, effective dye removal is observed as the pH of the solution rises (Pathania et al., 2017). The type of the adsorbent influences the increasing trend of MB removal with increasing pH. At lower pH, the percentage of MB removed decreased, whereas at higher pH, the trend of MB removal increased (Rahman et al., 2012).

2.10.2. Adsorbent dose

Adsorbent dosage is an important parameter because adsorbents provide the binding sites for dye adsorption. Therefore, adsorbent dosages determine the capacity of an adsorbent for a given initial concentration, separation cost and consequently the overall water treatment cost (Fan et al., 2017). The amount, size, and pore volume of adsorbent significantly influence the capacity of adsorption toward various molecules. The adsorbent's pore size and unoccupied site limit the rate and amount of dye molecules that can migrate to the surface. The removal

effectiveness grew significantly when the amount of adsorbent was raised until it reached a set amount of adsorbent, after which it dropped beyond the fixed adsorbent dose. Then, as the amount of adsorbent was increased, the removal efficiencies did not change considerably (Menya et al., 2018).

2.10.3. Adsorbate concentration

The adsorbate concentration is another crucial factor that influences the adsorption process. With increasing starting concentrations, the clearance effectiveness decreases. At low concentrations, most of the MB in a solution may come into contact with the adsorbent's active sites, but as the concentration rises, all MB species will be unavailable to contact the active surface due to active sites already being occupied (Rahman et al., 2012).

2.10.4. Contact time

Another crucial characteristic that has been discovered to have a major impact on the adsorption process is contact time. According to certain studies, dye removal efficiency increases fast up to 60 minutes, after which the adsorption rate gradually drops. This demonstrates that when the dye and adsorbent have enough contact time, the removal efficiency is higher until the equilibrium time is attained (Subramaniam et al., 2015).

Ho et al. (2005) demonstrated that as the dye concentration was increased, the adsorption capacity rose, and the rate of adsorption on the surface of the adsorbent had to be proportional to the driving force times the area. Within 30 minutes of contact time, a rapid initial dye removal was achieved, and adsorption capacity at equilibrium increased, but percent removal declined from 100 to 61 % as the MB dye concentration was varied. The equilibrium state was obtained with a further increase in contact time (Ho et al., 2005). According to Kaczmarski and Bellot, the quick removal of dye molecules was owing to solute transfer, as there were only adsorbate-adsorbent interactions with little interference from solute-solute interactions (Suresh Kumar et al., 2019).

3. MATERIALS AND METHOD

3.1. Materials

3.1.1. Chemicals and reagents

In this study: ferric chloride hexahydrate, $FeCl_3.6H_2O$ (Central Drug House, 99%) and ferrous chloride tetrahydrate, $FeCl_2.4H_2O$ (Central Drug House, 99%) were used as precursors of iron oxide nanoparticles. Sodium hydroxide, NaOH (LOBA CHEMIE PVT.LTD, 98%) and Hydrochloric acid (HCl) (LOBA CHEMIE PVT.LTD, 35.4%) was used to adjust the pH of the solutions. Phosphoric acid, H_3PO_4 (LOBA CHEMIE PVT.LTD, 37% (v/v) was used for chemical activation. HCl and distilled water were used to wash the activated carbon. Methylene blue, $C_{16}H_{18}ClN_3S$ (SAMIR TECH-CHEM, 82%) was used for stock MB solution preparation. In addition, dilute HCl and detergents were used for equipment cleaning and distilled water was used to prepare aqueous solutions and to rinse equipments.

3.1.2. Apparatus and equipments

The apparatus and equipments used for characterization of adsorbents during this research work were, Fourier transform infrared spectrometer (FT-IR) (FT/IR6600, JAPAN), X-ray diffractometer (XRD) (XRD-7000, UK), Scanning electron microscope (SEM) (JCM6000PLUS Bench Top SEM, JEOL, Japan), Thermal gravimetricAnalysis (HCT-1,CHINA), and UV-Vis spectrometer (UV-Vis-2000 AUG, USA). Sample collection materials (buckets, glass bottles and plastic bottles), digital electronic balance (FA2104, German), muffle furnace (MF2015, India), pH and conductivity meter (model Mettler-Toledo GmbH, JAPAN), oven, orbital shaker (3015,Germany), filter paper (Whatman 42), mortar and pestle, glass rod, pipettes, spatulas, Erlenmeyer flask, volumetric flask, different sizes of beakers were used for different activities.

3.2. Methods

3.2.1. Preparation of MB standard stock solution and working solutions

At room temperature, 1 g of MB dye was added to distilled water to prepare a stoke solution of 1000 mg/L in a 1000 mL volumetric flask. Then, the solution was wrapped with aluminum foil to prevent de-colorization of the solution as MB is naturally very sensitive to light. The

standard series solutions were prepared from the previously prepared stock solution by using the dilution method. UV-Vis spectrometer was used to measure the concentrations of MB dye solutions at the maximum absorbance of wave length of 665nm (Utomo et al., 2015).

3.2.2. Adsorbent preparation

3.2.2.1. Preparation and characterization of activated carbon (AC)

First, fruit pod‘s Waste fruit (seed) of Jacaranda mimosifolia was collected from ASTU‘s compound where JM trees are grown. Collected pods of JM were washed using distilled water to remove soluble impurities and, finally dried at 70^{o}C for 24 hrs. The biomass sample was then crushed and sieved to obtain 2 mm particle size using gravimetric sieve. These ground powder was stored in a desiccator for later use in both adsorption experiments and preparation of activated carbons (Serrano et al., 2014).

Second, previously ground 50 gram of powder of JM pod was weighed and then placed in a glass container and 50 ml of phosphoric acid, 37% (v/v) was added to form a homogeneous paste. The paste obtained was stirred at a temperature of 120℃ for a period of 8 hrs to increase the yield of the product. Afterwards, the samples were pyrolyzed at temperatures of 450℃, 550℃, and 650℃ in muffle furnace for 2 hrs. The muffle furnace temperature was programmed to increase at a rate of 10℃ ·min^{-1} then the produced AC was cooled for 4 hrs in a desiccator (Fan et al., 2017).

In the third and last stage, the activated carbon obtained was washed with 100 ml of concentrated hydrochloric acid, 37% (v/v) continuously with stirring for 6 hrs. Then the AC was washed with plenty of distilled water to remove the acid, any non-adhesive impurities and small particles, and dried at 105^{o}C in an oven. The dried AC was ground and passed through a 2 mm gravimetric sieve to attain the same particle size labelled as AC450, AC550, and AC650. Then, the AC was stored inside a sealed plastic container until use (Ferreira et al., 2017). The methylene blue adsorption efficiency of the synthesized ACs (AC450, AC550, and AC650) was investigated and AC550 was found to be more efficient than the other two ACs. Thus AC in this study refers to AC550.

3.2.2.2. Synthesis of Fe_3O_4 Nanoparticles

Magnetite nanoparticles were developed as follows. First, 1.99 g of ferrous chloride tetra hydrate (M.mass = 199) and 5.41g of ferric chloride hexahydrate (M.mass = 270.5) was dissolved into a 150 mL conical flask with 50 mL distilled water to make a 2:1 M ratio and 20 mL of the ammonia solution was added into the same solution to obtain a brown colloidal solution under sonication for 20 minutes. Ammonia solution is used as a precipitating agent in the synthesis of magnetite to obtain the most appropriate moles ratio of Fe (III) and Fe (II) and to achieve the best characteristics of magnetite. Then, a freshly prepared 0.5 M NaOH solution was added drop-wise to the above mixture under continuous stirring at 500 rpm to adjust the pH to11. The solution was refluxed for 1 hr with continuous stirring at 70^oC to homogenize the solution and also for the completion of the reaction. After that, the synthesized Fe_3O_4 NPs were separated by using a bar magnet and washed three times by using distilled water. The separated Fe_3O_4 NPs were dried in an oven at around 105^oC for 24 hrs. The dried sample was stored in an airtight container for further analysis (Yew et al., 2016).

3.2.2.3. Synthesis of AC-Fe_3O_4 Composite

In brief, AC-Fe_3O_4 nanocomposites were prepared from Fe_3O_4 nanoparticles and activated carbon with1:1, 2:1 and 3:1 volume ratios of activated carbon to Fe_3O_4 samples in 150 mL distilled water under sonication for 30 minute in a 250 mL flask (Bagheri et al., 2017). Under vigorous magnetic stirring at 80^oC for 0.5 hr, 0.2 M NaOH solution was added drop wise into the above suspensions until the pH increased up to 10. Then the mixtures continuously stirred at 550 rpm for 1 hr at 80^oC. Finally, the product was washed with distilled water and absolute ethyl alcohol repeatedly and then dried at 105^oC overnight. The dried composites were ground and passed through 0.18 mm sieve to attain same particle size labelled as MAC1:1, MAC2:1, and MAC3:1. Then, the MAC was stored inside a sealed plastic container until use. The MB adsorption efficiency of the synthesized composite samples were investigated and it was found that 2:1 ratio of activated carbon to Fe_3O_4 sample had the highest adsorption capacity (Joshi et al., 2019).

3.2.3. Characterization of AC, Fe_3O_4 NPs, and AC-Fe_3O_4 nanocomposite

In this thesis the synthesized nanoparticles; Fe_3O_4 NPs, AC, and AC-Fe_3O_4 composite were characterized by Fourier-transform infrared spectroscopy (FTIR), X-ray diffraction (XRD), Scanning electron microscope (SEM), and Thermal gravimetric analysis (TGA) methods.

3.2.3.1. Fourier-transform infrared spectroscopy (FTIR) characterization

The FTIR spectra of Fe_3O_4 NPs, AC, and AC-Fe_3O_4 composite were recorded the spectrometer in the range of 400 – 4000 cm^{-1} using the KBr disc method.

3.2.3.2. X-ray diffraction (XRD) characterization

The XRD of the nanoparticles and the composite adsorbents were tested at ASTU research laboratory of Material Science and Engineering Department using an X-ray diffractometer. The mass of approximately 0.5 g of the nanoparticles and the composite samples were measured for XRD characterization and filled in a sample holder. Then the sample was analyzed by using an X-ray diffractometer with Cu-Kα radiation source at λ= 1.5418 Å and operating at 40 kV and 30 mA. X-ray diffractograms of Fe_3O_4 NPs, activated carbon, and AC-Fe_3O_4 Composite were obtained for the 2θ angles scan range from 10˚ to 80˚ with a scan speed of 3˚/ min, and a counting time of 0.40 sec.

3.2.3.3. Scanning electron microscope (SEM) characterization

The Fe_3O_4 NPs, AC, and AC-Fe_3O_4 Composite were characterized by a scanning electron microscope using a high-energy electron, and the out coming electrons are analyzed by applying a 10 kV electron acceleration voltage. These coming electrons give information about morphology, composition, the orientation of grains, and crystallography information of material. It provides information about the surface features and texture, shape, size, and arrangement of the particles on the sample surface (Gunarathne et al., 2018, S. K. Sharma et al., 2018). For SEM, 10 mg sample of the nanoparticles and the composite were measured from the previously prepared sample and characterized by using scanning electron microscope.

3.2.3.4. Thermal gravimetric analysis (TGA)

Thermogravimetric experiments were carried out by a thermogravimetric analyzer (SHIMADZU, TGA-50) in order to determine the pyrolysis behavior of AC and AC-Fe_3O_4 composite. TGA records the weight loss as a function of temperature. The thermal degradation behavior of the AC and AC-Fe_3O_4 composite adsorbent was observed with a Thermobalance detector, TGA-60H (Model No: C30575100456TK, Korea). Approximately 15.463 mg of test sample was loaded into the crucible for analysis in the equipment. The experiment was carried out in an inert environment obtained by continuous flow of 50 mL/min of nitrogen gas that was used as non-oxidizing agent in order to determine the thermal stability of the AC and AC-Fe_3O_4 composite. The AC and AC-Fe_3O_4 composite adsorbent was heated from 25^oC to 900^oC at a heating rate of 15^oC/min.

3.2.4. Batch Adsorption Experiments

Prior to batch adsorption experiment to optimize the factors that affect the adsorption process, pre-test adsorption experiment at optimized working condition was performed. The pre-test experiment was conducted to selected the best adsorbent material among the three different proportions of activated carbon and Fe_3O_4 NPs (1:1, 2:1, and 3:1, respectively). As indicated in (Appendix 1) the pre-test experiment was conducted based on available literature by performing batch adsorption experiment at pH 7, dose of 0.2 g/50ml, contact time of 30 min, initial concentration of 10 mg/L, shaking speed of 150 rpm at room temperature (Cazetta et al., 2016). The criterion utilized to specify the best proportion is the highest value of adsorption capacity to remove MB from contaminated water (Appendix 1).

All adsorption experiments were carried out in batch mode because of the simplicity and reliability of the technique for small-scale investigations (Sharma et al., 2017). Batch mode adsorption studies for individual parameters were carried out using a 250 mL beaker and the parameters such as MB initial concentration, adsorbent dose, contact time, and pH were studied by adjusting the pH of the solution by 0.1 N HCl and 0.1 N NaOH solutions (Raposo et al., 2009). After each batch adsorption experiment is completed using selected AC-Fe_3O_4 Composite adsorbent, the resulting suspension was taken and filtered using a Whatman filter paper (42) then the filtrate was analyzed for the corresponding MB dye concentration using UV-Vis spectrophotometer (UV-Vis-2000 AUG, USA) at the maximum wavelength of 665

nm (Ibrahim et al., 2021). Then, the percent adsorption efficiency (% R) and the adsorption capacity (milligram of dye adsorbed per gram of adsorbent (qe)) were calculated using Equations 7 and 8, respectively.

$$\%R = \frac{C_{0-C_e}}{Co}\, x\, 100 \quad \ldots\ldots\ldots\ldots\ldots\ldots\ldots\ldots\ldots\ldots\ldots\ldots\ldots\ldots\ldots\ldots (7)$$

Where, % R is percent removal, Co is initial dye concentration (mg/L), and Ce is concentration after adsorption (mg/L).

$$q_e = \frac{C_{0-C_e}}{m} xV \ldots\ldots\ldots\ldots\ldots\ldots\ldots\ldots\ldots\ldots\ldots\ldots\ldots\ldots\ldots\ldots\ldots\ldots\ldots\ldots\ldots\ldots (8)$$

where, q_e is the MB dye quantity adsorbed at equilibrium (mg/g), Co is initial concentration of MB dye (mg/L), Ce is the equilibrium MB concentration in solution after adsorption, m is adsorbent mass in gram and V is volume of MB dye solution (L) used during the experiment (Vunain et al., 2017). During the adsorption process; dissolved species are transported into the porous adsorbent particle by diffusion and are then adsorbed onto the extensive inner surface of the adsorbent.

3.2.4.1. Effect of pH

The effect of initial pH of the solution was investigated at various pH (3, 5, 7, 9, and 11) and making other parameters fixed. 0.2 g of AC-Fe_3O_4 composite adsorbent was added to 50 ml of 10 mg/L MB dye aqueous solution. The mixtures were stirred at 150 rpm for a constant adsorption time of 1 hr. After completion of adsorption time the adsorbent was removed from the solution and the concentration of residual methylene blue in each solution was determined using UV-VIS spectrometer, and percent removal efficiency and adsorption capacities were calculated (Sánchez-Martín et al., 2010).

3.2.4.2. Effect of adsorbent dose

50 ml of 10 mg/L MB dye solution was mixed with various dosages of AC-Fe_3O_4 composite adsorbent (0.025, 0.05, 0.075, 0.1 and 0.2 g) at a contact time of 1 hr, stirring rate of 150 rpm, temperature of 25^{o}C and the pH value kept at the optimized value. After this, the residual MB dye concentration which remains in the filtrate was measured by UV-Vis spectrophotometer, and then percent removal efficiency and adsorption capacities were calculated for different dosages (Raposo et al., 2009).

3.2.4.3. Effect of contact time

The optimized amount of the AC-Fe_3O_4 adsorbent was added to 50 ml of 10 mg/L MB dye solution for various contact times (5,10, 15, 30, and 60 minutes) at the optimized pH, stirring rate of 150 rpm and temperature of 25^oC. After the specified time, the residual MB dye concentration which remains in the filtrate was measured by UV-Vis spectrophotometer (Sudha et al., 2007).

3.2.4.4. Effect of initial concentration of methylene blue

The optimized amount of the AC-Fe_3O_4 adsorbent was added into different beakers with 50 ml volume of MB dye solution. The initial concentrations of the dye solutions were (10, 50, 100, 150 and 200 mg/L). The pH and contact time was adjusted to the optimized values with the stirring rate of 150 rpm and the temperature at 25^oC. The mixture was agitated and after the specified time, the filtrate concentrations of MB dye were analyzed using a UV-Vis spectrophotometer (Sudha et al., 2007).

3.2.5. Kinetic and Isotherm Study of Adsorption

Both kinetic and isotherm studies were carried out to determine the adsorption mechanism that occurred through the adsorption process. Effect of MB dye adsorption kinetics was determined by varying the contact time as: 5, 10, 15, 30, and 60 minutes by keeping all parameters (pH, adsorbent dose, and initial MB concentration) at optimized value. It was evaluated by using 0.1 g of adsorbent and placed in 250 mL Erlenmeyer flasks, each containing 50 mL of 50 mg/L MB solution. The pH of the solution was maintained at the optimized value. The flasks were stoppered and continuously shaken at a speed of 150 rpm. The sample solution was immediately filtered of and then analyzed for MB equilibrium concentration. The samples were collected at various time intervals. The equilibrium data were fitted to pseudo-first-order (eqn.2) and pseudo-second-order (eqn.3) model equations. Satisfactory conformity between experimental data and the model-predicted values were expressed by the correlation coefficient (R^2).

MB adsorption isotherms were determined by varying the initial MB concentration from 10 to 200 mg/L while keeping all other parameters (pH, adsorbent dose, and contact time) at optimized conditions. In separate flasks, 50 mL of solutions containing different amounts of

initial MB concentration (10, 50,100,150 and 200 mg/L) were added. After the reaction period, all samples were filtered and analysed for the corresponding MB concentration. The equilibrium data were fitted to the Langmuir (eq.4) and Freundlich (eq.6) isotherm models to determine the relationship between the adsorption capacity and the MB concentration in solution at equilibrium. Equilibrium isotherm equations are used to describe the experimental adsorption data which provide information about the capacity of the adsorbent or the amount required for removing a unit mass of pollutant under the system concentrations. Linear regression is frequently used to determine the best-fitting isotherm, and the applicability of isotherm equations is compared by judging the correlation coefficients. The amount of MB adsorbed onto the composite at the equilibrium (q_e) was calculated by using equation 8 (Gao et al., 2013).

3.2.6. Reusability of Synthesized AC-Fe_3O_4 Composite

The reusability of the used adsorbent, AC-Fe_3O_4 nanocomposite was investigated by performing six successive adsorption-desorption cycles of methylene blue on the AC-Fe_3O_4 adsorbent by using 0.1 M HCl desorption solution. The adsorption of methylene blue by 0.1 g of AC-Fe_3O_4 adsorbent at pH of 7, initial MB concentration of 50 mg/L, 150 rpm agitation speed, and contact time of 15 minutes at 25 °C was performed, followed by desorption of adsorbed MB with 0.1 M HCl solution after each cycle. After 15 minutes of adsorption of 50 mg/L MB solution by the nanoadsorbents, MB desorption experiments was conducted by reacting the recovered adsorbents in 50 mL of 0.1M HCl desorption solution on a shaker for 15 minutes at room temperature. The supernatant sample was withdrawn for analyzing the MB desorption efficiency. Then magnetic adsorbent was separated, washed and dried at 60^0C for 2 hrs.

The reusability of the regenerated adsorbent was calculated for the above adsorption-desorption experiments of six times. In order to assess the possibility of recycling the adsorbent, the percentage of MB desorbed to adsorb was calculated. Desorption efficiency was calculated by the equation:

$$Desorption\ efficienc(\%) = \frac{C_{desorbed}}{C_{adsorbed}}\ x\ 100 \qquad (9)$$

Where $C_{desorbed}$ is the amount of the MB that is removed from the loaded powder after desorption study, $C_{adsorbed}$ is $C_0 - Ce$ for each recovery process, C_0 is the initial MB concentration, and Ce is the equilibrium MB concentration in mg/L (Ahmed et al., 2019, Y. Chen et al., 2020).

4. RESULTS AND DISCUSSIONS

4.1. XRD Analysis

The XRD pattern of the selected AC (AC550), Fe_3O_4NPs and AC- Fe_3O_4 nanocomposite are shown in Figure 11. The XRD patterns of the prepared AC550 showed a broad reflection at approximately 23.2º in 2θ which is suggestive of an amorphous carbon attributed to the typical 002 planes of crystalline graphite structure produced during the carbonization process (X. Wang et al., 2017, Moosavi et al., 2020, Koilraj & Sasaki, 2017). The AC550 sample has small humps at 2θ of 14.3°, 29.8°, 35.04, and 37.8° and these peaks are attributed to the cellulose presented in crystalline form. Furthermore, the peak's width is attributed to the presence of other organic matters such as lignin and hemicellulose (Nanda et al., 2013, Sharma et al., 2017, Vassilev et al., 2012). Amorphous carbon was the main phase present in the materials, which corresponds to disorganized structures and may be favorable to adsorption since the empty spaces that favor the accommodation of adsorbate molecules on the adsorbent surface (Ã. Crini et al., 2008). Similar XRD patterns were also observed in activated carbon produced from peanut shells (Georgin et al., 2021).

The crystal structure of the synthesized Fe_3O_4 nanoparticles was evidenced by the diffraction peaks, with the strong ones appearing at 2θ values of 21.22, 30.3, 35.74, 43.5, 53.46, 57.6 and 63.10 respectively. The peaks at 2θ of 30.3, 35.74, 43.5, 57.6 and 63.10 are characteristics of the 220, 311, 400, 422, 511 and 440 basal planes of the crystalline magnetite portion of the materials respectively (Cazetta et al., 2016, Xiaoduo Liu et al., 2019, Raj et al., 2015). These results corresponds to the standard pattern for cubic magnetite (JCPDS No.19-0629) (Bagheri et al., 2017, Daneshvar Tarigh et al., 2013, Zhou et al., 2014). The diffraction peaks revealed that the obtained products were pure spinel phase magnetite Fe_3O_4 nanoparticles (Yuvakkumar et al., 2014, Solomon et al., 2012). Similar findings was reported for magnetite nanoparticles with intensity of the diffraction peaks at 2θ of 35°, 57° and 63° corresponding to the 311,511 and 440 planes of the magnetite Fe_3O_4 structure (JCPDS 75-1609) (Yang et al., 2015;Viju Kumar et al., 2018). The average crystallite size of Fe_3O_4 in the composite material was calculated as 9.789 nm from XRD pattern by using the Scherrer formula (eq 1) (Raj et al., 2015).

Table 1: Peak positions and crystalline size of the synthesized Fe_3O_4 NPs.

Peak position(2θ)	FWHM	Crystallite size D (nm)	Average size (nm)
21.21694	0.63656	12.69704	9.78923
30.29314	0.86443	9.52095	
35.76288	1.48044	5.63854	
43.35691	0.63826	13.39413	
53.64737	1.22829	7.24761	
57.35937	0.8111	11.16411	
63.01261	1.05142	8.86221	

For the AC- Fe_3O_4 nanocomposite material, , apart from the (0 0 2) reflection from activated carbon, many small peaks are observed in the XRD pattern and all of them correspond to the peaks of Fe_3O_4 as evidenced from the comparison of the simulated pattern of Fe_3O_4. The AC-Fe_3O_4 nanocomposites possess dominant peaks which were also shown in the magnetite nanoparticles. Additionally the XRD of AC- Fe_3O_4 composite shows a peak at 2θ value of 77.68° which were shown on XRD pattern of AC550 but more intensified in the composite. Diffraction peaks at 2θ = 14, 23, 30, 35, 43, 57, and 63 and 77 were mainly observed in the synthesized composite which also exist in the synthesized AC and Fe_3O_4 nanoparticles. The presence of both Fe_3O_4 and AC diffraction peaks in the nanocomposite indicates a crystalline nature of AC-Fe_3O_4 composite (Xiaoduo Liu et al., 2019, Mazloumi et al., 2009). This indicates that magnetite nanoparticles are loaded on the surface of the activated carbon since the composite is less crystalline than the magnetite nanoparticles (Lai et al., 2016). By using Scherer formula eq (6), the calculated average crystallite size of the synthesized AC-Fe_3O_4 composite was found to be 9.72 nm (Raj & Joy, 2015).

Table 2: Peak positions and crystalline sizes of the synthesized AC-Fe_3O_4 nanocomposite.

Peak position(2θ)	FWHM	Crystallite size D (nm)	Average size (nm)
21.02089	0.43807	18.44421	9.72059
24.46298	9.27347	0.87656	
29.92109	0.35691	23.03947	
33.15649	0.47096	17.59989	
35.69674	1.84645	4.52001	
43.44566	1.24333	6.87796	

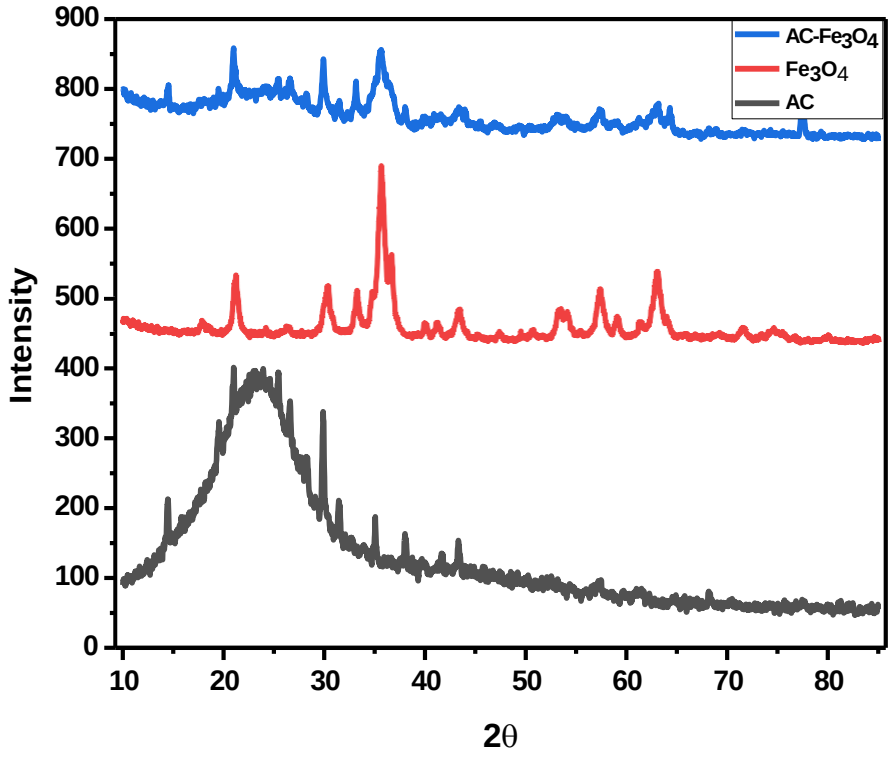

Figure 9**:** XRD pattern of AC, Fe_3O_4NPs, and AC-Fe_3O_4 nanocomposite**.**

4.2. FTIR Analysis

Fourier transform infrared (FTIR) spectra of the precursors, AC550, Fe_3O_4, and the composite AC-Fe_3O_4 are shown in Figure 12. All of the materials showed a broad band at 3406 cm^{-1} that corresponds to the O-H stretching vibration mode of surface-adsorbed water molecules (Boonamnuayvitaya et al., 2005, Bagheri et al., 2017, Ren et al., 2011, Li et al., 2012). The bands at 2921 and 2855 cm^{-1} correspond to the aliphatic C-H stretching vibration mode (Boonamnuayvitaya et al., 2005, Spessato et al., 2019). A small band observed at 1602 cm^{-1} is assigned to the stretching aromatic C=C vibration mode and band at 1452 cm^{-1} corresponds to asymmetric –C-H stretching which may be caused by the presence of ester, ether, carbonyl, or aromatic functional group on the surface of nanomaterials (B. Chen et al., 2011, Boonamnuayvitaya et al., 2005). Moreover, the stretching vibration of C-O located at 1089 cm^{-1} is assigned to the carboxylate group(-COOH) which may originate from organic compounds (X. Liu et al., 2019, Koilraj et al., 2017). A characteristic peak at around 563 cm^{-1} corresponds to the Fe-O stretching band of magnetite (Fe_3O_4). This small sharp peak confirms the presence of Fe_3O_4 NPs. Characteristic peaks as the peaks lying in the region between 400 and 600 cm^{-1} were corresponding to Fe_3O_4 (B. Chen et al., 2011; Viju Kumar et al., 2018;Yuvakkumar et al., 2014). The FTIR results clearly indicate that the Fe_3O_4 nanoparticles have been loaded into the AC (Xiaohuan Liu et al., 2019, Solomon et al.,2012, Raj et al., 2015).

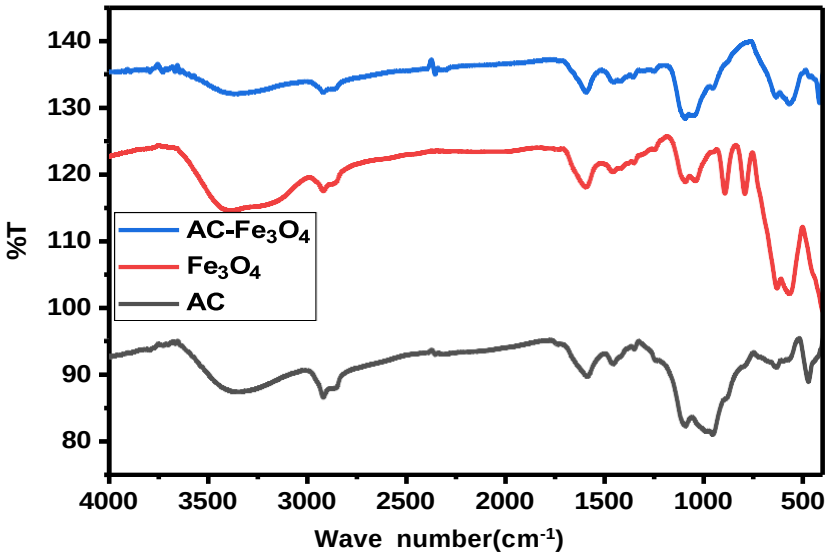

Figure 10: FTIR spectra for the AC550, Fe_3O_4, and AC-Fe_3O_4 Composite

4.3. SEM Analysis

Surface morphology of the AC550, , Fe_3O_4, and AC-Fe_3O_4 Composite were examined by using scanning electron microscopy (SEM) to investigate the shape, size, and porosity of the materials as shown in Figure 13. The SEM image of AC (Figure 13-A) shows that the adsorbent developed from JM has high porous structure full of cavities like honeycomb structure. These meso- and micropores of AC act as a main role of pollutant adsorption like dyes or heavy metals or other pollutants in water. According to these results and other literatures, the high porosity and high surface area are very important factors to achieve high adsorption capacity. The concentration of these pores and surface area can be enhanced using methods of activation. The pyrolysis temperature (550^0C) makes volatilization more subtle, making the AC porous and creating small voids within the AC matrix. The micrographs also clearly show that the surface of the AC is rough and porous; therefore it is good candidates as adsorbents. Similar kind of SEM result was obtained by Zhang et al. (2015) who prepared AC from peanut shell (S. Zhang et al., 2015, Moosavi et al., 2020).

The SEM images of Fe_3O_4 NPs (Figure 13B) crystallites are nearly square in shape and it can be seen that the particles agglomeration, indicating a good connectivity between the grains together and the size. Additionally some porosity is observed in SEM image of Fe_3O_4 NPs which helps for adsorption proprieties of materials. The SEM image of the AC-Fe_3O_4 (Figure 13C) composite has a larger particle size and homogeneous surface than the precursor materials. The composite adsorbent had irregular rough surface structure, with larger pore size, and pore volume, which indicates that the material possesses good characteristics to be employed as an adsorbent for MB dye uptake. Figure 13C shows the SEM image of AC-Fe_3O_4 composite, from which it can be seen that Fe_3O_4 nanoparticles are sufficiently loaded on the activated carbon , and aggregation occurred due to the magnetic properties of Fe_3O_4, leading to the uneven distribution of Fe_3O_4 on the surface of the activated carbon (Y. Wang et al., 2021). The SEM image in Figure 13C showed that the AC-Fe_3O_4 composite has a more compact structure than the activated carbon as well as the magnetite. A close investigation of the surface structures the AC-Fe_3O_4 composite (Figure 13C), shows that the whole rough surface is stacked by multilayer nanoparticles aligned irregularly in different dimensions (Xie et al., 2014; Aghazadeh et al., 2011; Zheng et al., 2021). Adsorbents with high surface area and small particle size increase the adsorption (Moosavi et al., 2020).

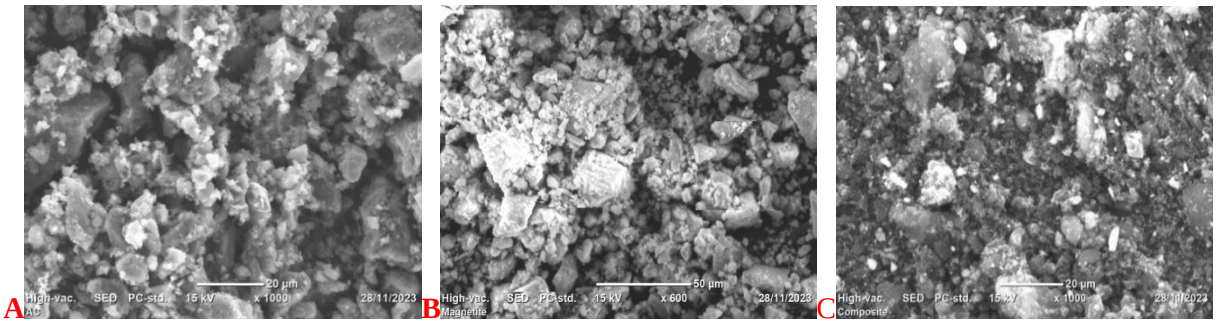

Figure 11**:** SEM images of AC550 (A), Fe_3O_4 NPs (B) and AC-Fe_3O_4 Composite (C).

4.4. TGA Analysis

Figure 14 shows the weight loss curves of the two samples: AC and AC-Fe_3O_4 composite by weight in N_2 atmosphere and at a 15^oC/min heating rate. From the thermogravimetric graph, the maximum thermal degradation temperature of the AC-Fe_3O_4 composite adsorbent was around 500^oC. Thermal decomposition of AC-Fe_3O_4 composite adsorbent occurred in three stages. First stage of the decomposition occurred at a temperature of 50^oC which corresponded to an initial weight loss of around 0.5% or around 0.077 mg. This may be due to the moisture evaporation or low molecular weight volatile compounds (Boonamnuayvitaya et al., 2005, Saadatkhah et al., 2020, Ramos Filho et al., 2005). Second stage of the decomposition contributed to a major weight loss of about 2.302 mg at a temperature of 550^oC. This weight loss is around 14.887% of the total initial weight, may be due to the decomposition of the adsorbent into other forms by releasing carbon dioxide or carbon monoxide gases. This result implies that both AC and AC-Fe_3O_4 composite adsorbents have low thermal stability above 550^oC. In the final stage, from temperature range of 650-900^oC, the weight loss curve was almost flat. There is no decomposition of AC-Fe_3O_4 composite adsorbent at this temperature range. This may be because the adsorbent was converted into non-volatile inorganic ashes (Saadatkhah et al., 2020). Thus the suitable working temperature of the AC-Fe_3O_4 composite adsorbent should be below 500^oC since the composite is more stable at this temperature range. On the basis of the performed thermogravimetric analyses, it can be stated that the AC-Fe_3O_4 composite adsorbent has high heat resistance characteristics (Boonamnuayvitaya et al., 2005, Buketov et al., 2014).

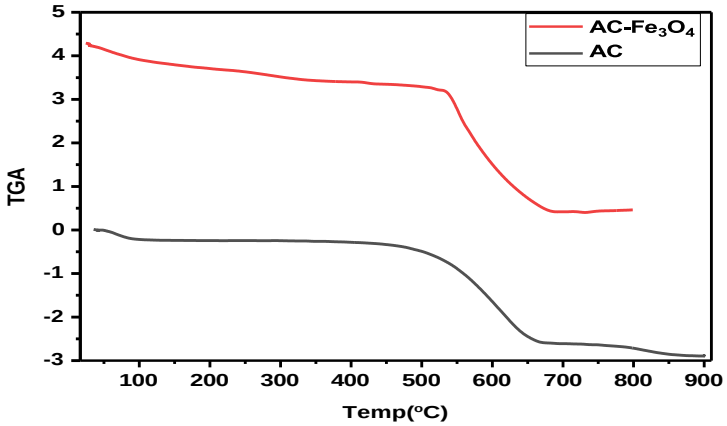

Figure 12**:** TGA plots of AC and AC-Fe_3O_4 Composite adsorbent (initial heating rate is 15^0C/min).

4.5. Optimization of Working Parameters for the Removal of MB from Wastewater

4.5.1. Effect of pH

The effects of pH on the MB adsorption by AC-Fe_3O_4 Composite adsorbent was studied over a wide pH range from 3 up to 11, at an initial MB concentration of 10 mg/L. According to the results shown in Figure 15, it is obvious that the adsorption of MB on the AC-Fe_3O_4 composite adsorbent was strongly pH-dependent. It shows that the MB removal extents of the adsorbent gradually increase when pH increases from 3(96.99%) to 9(99.23%), while the removal extents starts to remain almost constant from pH 9 onwards. This implies that pH around 9 is found to be the optimum pH in which the maximum uptake of MB dye was obtained. As the pH increases, it is usually expected that the cationic dye adsorption also increases due to increasing of the negative surface charge of adsorbents. With increasing pH values the adsorption of MB on AC-Fe_3O_4 composite tends to increase. The maximum adsorption capacity at a pH of 9 is 5.08 mg/g. The low adsorption of MB at an acidic pH was suggested to be due to the presence of excess H^+ ions that compete with the MB dye cation for adsorption sites. The number of positively charged sites decreases while the number of negatively charged sites increases, favouring the adsorption of MB which can be explained by the electrostatic interaction of cationic dye species with the negatively charged adsorbent surface. The dye removal efficiency remains the same as the pH value increased from 9 to 11 is due to the formation of a hydroxyl complex between the adsorbent and the dye. This

phenomenon was similar to previous result reported by different studies (Sánchez-Martín et al., 2010, El-Tokhy et al., 2020).

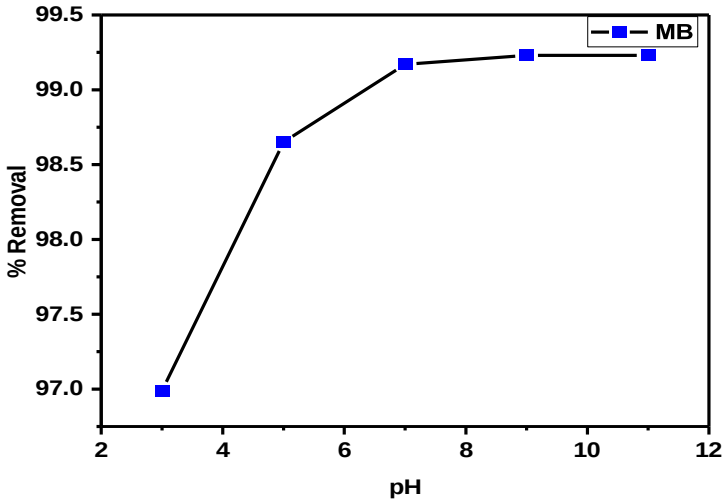

Figure 13**:** Effect of pH on the removal of MB

4.5.2. Effect of Adsorbent dosage

Figure 16, shows the MB removal efficiency and adsorption capacity, respectively of AC-Fe_3O_4 composite adsorbent under different adsorbent dosage (0.05, 0.075, 0.1, 0.25 and 0. 5 g) by keeping other parameters constant per 100 mL volume of adsorbate solution. The results showed that the percent removal of MB by the AC-Fe_3O_4 composite adsorbent was increased from 84.36 % to 97.95% with an increase in AC-Fe_3O_4 composite dosage from 0.05 to 0.25 g. This increase in percent removal with an increase in AC-Fe_3O_4 composite adsorbent dose may be due to the increase in surface area of the adsorbent and more adsorption sites are available to absorb the MB from the water sample (Adegoke et al., 2015). Increased adsorbent dosage implied a greater surface area and a greater number of binding sites available for the constant amount of MB. Then the removal percent of MB by AC-Fe_3O_4 composite adsorbent slightly increases with the increase in adsorbent dosage from 0.25 to 0.5 g. This result is in an agreement with the findings of MB adsorption to other activated carbon-based adsorbents (P. Wang et al., 2014, Gao et al., 2013). Thus, the optimized adsorbent dose (0.25 g) was maintained at in all the subsequent experiments, which was considered to be sufficient for the

removal of MB. Therefore, as shown in Figure 16, the percent removal (%) of MB initially increased sharply with increasing AC-Fe_3O_4 composite adsorbent dose. The maximum adsorption capacity at 0.1 g of nanocomposite dose is 9.72 mg/g.

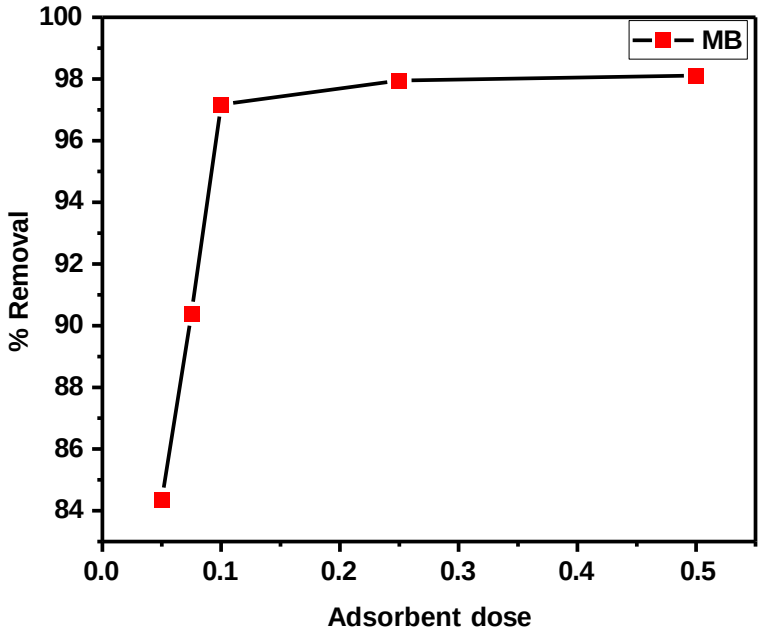

Figure 14**:** Effect of adsorbent dose on the removal of MB

4.5.3. Effect of contact time

Figure 17 shows the MB removal efficiency and adsorption capacity of the AC-Fe_3O_4 composite under different contact time (5, 10, 15, 30, and 60 min) and other parameters kept constant per 100 mL volume of adsorbate solution. The results showed that the percent removal of MB by the AC-Fe_3O_4 composite adsorbent increased from 69.85 % to 98.10 % with an increase in contact time from 5 to 15 minutes. An increase in removal efficiency up to 15 minutes is due to strong forces of attraction between the positive sites of cationic dyes and the adsorbent surface. Comparable result was found by (Adegoke et al., 2015). Then the removal percent of MB by the AC-Fe_3O_4 composite adsorbent almost remains constant with the increase in contact time from 15 to 60 minutes. This phenomenon is attributed to the fact that a large number of vacant surface sites are available for adsorption at the initial stage, and after a lapse of time, the remaining vacant surface sites are difficult to be occupied due to repulsive force between the solute molecules on the solid and bulk phase (Nasr et al., 2017).

Therefore, contact time of 15 min is found to be the optimum time in which the maximum uptake of MB dye was obtained. The maximum adsorption capacity at that specified contact time was 9.81 mg/g (Figure 17).

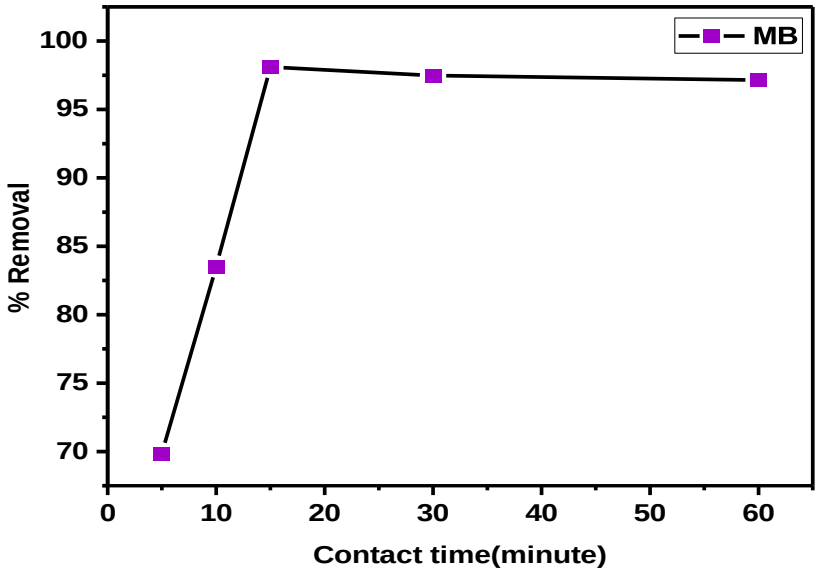

Figure 15*:* Effect of contact time optimization on the removal of MB

4.5.4. Effect of initial concentration

Figure 18 shows the MB removal efficiency and adsorption capacity of the AC-Fe_3O_4 nanocomposite adsorbent under different initial MB concentration of 10, 50, 100, 150, and 200 mg/ While keeping the other parameters constant per 100 mL volume of adsorbate solution. The results showed that the removal percent of MB increased from 99.73 % to 99.98 % with an increase in initial MB concentration from 10 to 50 mg/L. Then the percent removal of MB by the AC-Fe_3O_4 composite adsorbent decreased with the increase in initial MB concentration from 50 to 200 mg/L. Further increase in MB concentration results a decrease in percent removal due to the lack of active sites of the AC-Fe_3O_4 composite adsorbent (Sudha et al., 2007). This implies initial MB concentration of 50 mg/L is found to be the optimum initial concentration in which the maximum uptake of MB dye was obtained. It means that the adsorption is highly dependent on the initial concentration of dyes (Adegoke et al., 2015). The maximum adsorption capacity at initial MB concentration of 50 mg/L is 49.98

mg/g (Figure 18). The results obtained in this study are consistent with the results obtained by (Sudha et al., 2007).

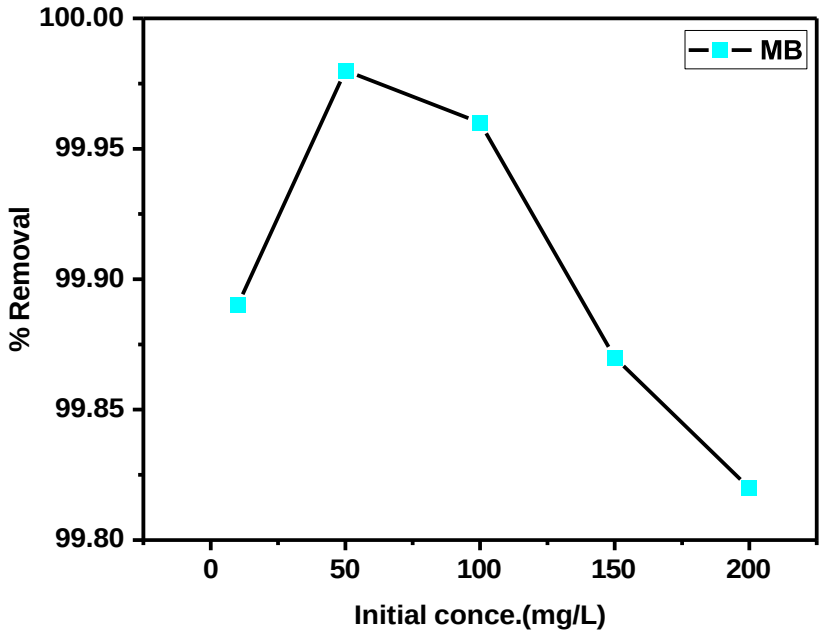

Figure 16*:* Effect of initial concentration of MB

4.6. Kinetics Study

Kinetics studies help to select optimum operating conditions for the full-scale batch process which have been applicable to investigate the mechanism of adsorption and potential rate controlling steps. To further understand the characteristics of the adsorption process, the pseudo-first and second-order kinetics order kinetic models were applied to fit experimental data obtained from batch experiments. The conformity between experimental data and the model-predicted values was expressed using the correlation coefficient significance. The greater degree of fit with the experimental value is the more applicable model to the kinetic study. The kinetics study were done at pH of 9, initial MB concentration of 50 mg/L, adsorbent dosage of 0.25 g, agitation speed of 150 rpm at room temperature. The MB uptake was very rapid in the first 10 minute and adsorption equilibrium was achieved in 15 minute similar to other adsorbent studies (B. Wu et al., 2017, Song et al., 2020).

4.6.1. Pseudo-first order kinetic model

To determine whether the adsorption process fits with the pseudo-first-order model or not, the experimental data using contact time ranging from 5 to 60 min and pH of 9, initial MB concentrations of 50 mg/L, adsorbent dosage of 0.25 g at room temperature, and 150 rpm agitation speed were introduced to Equation 2. From the slopes and intercepts of pseudo-first order model [Log (qe-qt) versus t] (Figure 19), the pseudo-first order rate constant, k_1 and equilibrium adsorption density, qe were determined (Y. Wang et al., 2021). The kinetic parameters obtained from the models are given in Table 3. The qe and correlation coefficient (R^2) values calculated using pseudo-first order model were found to be 10.66 mg/g and 0.77182 respectively. This indicates that there is great variation between calculated (10.66 mg/g) and theoretical (49.94 mg/g) qe values. Thus the experimental data could not be well described by pseudo-first order model.

Table 3: Results of line fit model of pseudo-first order kinetic.

Pollutant	Co(mg/L)	qe,exp(mg/g	qe,cal(mg/g)	R^2	Slope	Intercept
MB	50	49.94	10.66	0.7718	-0.0194	-0.2980

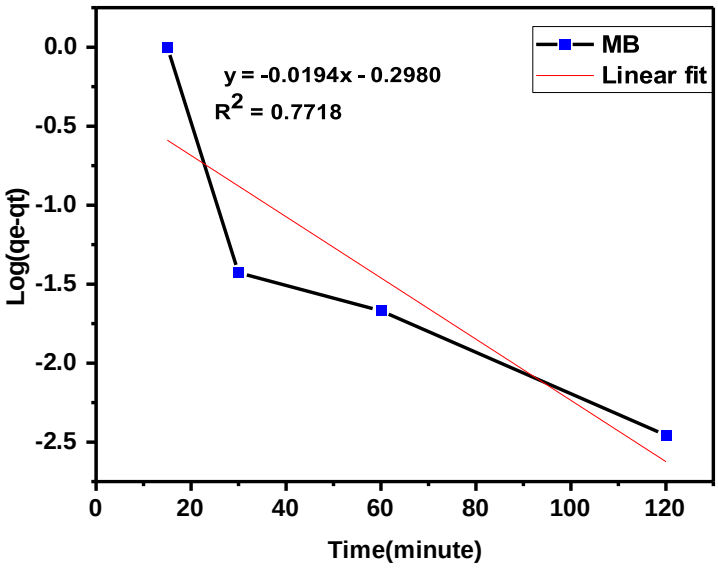

Figure 17*:*Pseudo-first order kinetic plot for the adsorption of MB onto AC-Fe_3O_4 Composite adsorbent.

4.6.2. Pseudo-second order kinetic model

In addition to the pseudo-first-order kinetics model, the linearized form of the kinetic rate expression for a pseudo-second-order model was applied to the experimental data. Calculated equilibrium adsorption capacity q_e (cal), pseudo-second-order rate constant (K_2), and the correlation coefficient (R^2) were obtained from the model using Equation 3. The linear plots of t/qt against time are shown in Figure 20 for MB adsorbed on AC-Fe_3O_4 composite adsorbent. From the slope and intercept of pseudo-second order model, t/qt versus t (Figure 20), the value of qe and K_2 were determined. The kinetic parameters obtained from the models are given in Table 4. Pseudo second-order reaction rate model which give a linear relationship adequately described the kinetics of adsorption of MB with high correlation coefficient (R^2 = 1) and its theoretical equilibrium capacities qe (exp) (49.94 mg/g) fit well with the calculated qe (50 mg/g) data. Figure 20 and Table 4 showed the value of R^2 on pseudo-second-order for MB is higher than on pseudo-first-order kinetics and the calculated adsorption capacity qe (cal) was closer to the experimental adsorption capacity qe(exp), indicating that the pseudo-second-order kinetic model describes the adsorption process of MB by AC-Fe_3O_4 composite adsorbent perfectly. The result indicates that the adsorption perfectly obeys the pseudo-second-order model meaning the controlling rate step is chemisorption. Meanwhile, the result showed that the rate of adsorption depended on the availability of adsorption sites on the surface of adsorbent rather than MB concentration in bulk solution (Y. Liu et al., 2008). A similar fit to this model has also been reported (Gao et al., 2013, Y. Zhang et al., 2020).

Table 4: Results of line fit model of pseudo – second order kinetics.

Pollutant	Co(mg/L)	qe,exp(mg/g)	qe,cal(mg/g)	R^2	Slope	Intercept
MB	50	49.94	50	0.9989	0.020	1.446

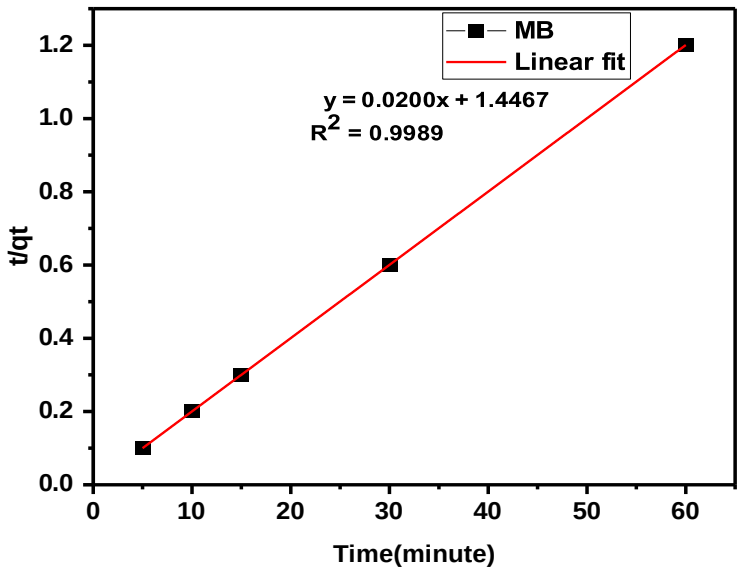

Figure 18*:*Pseudo-second order kinetic plot for the adsorption of MB onto AC-Fe_3O_4 composite adsorbent.

4.7. Adsorption Isotherm

The adsorption equilibrium provides important physicochemical data for evaluating the applicability of the adsorption process as a unit operation. In this study, the equilibrium data were analyzed by using Langmuir and Freundlich isotherm models. These are generally related to the type of coverage, the possibility of interaction between the adsorbent and adsorbate species, the heterogeneity and homogeneity of the adsorbent (Senthil Kumar et al., 2010). Isotherm models relate adsorbate per unit weight of adsorbent (qe) to the equilibrium adsorbate concentration in the bulk fluid phase Ce. This helps to optimize the design of an adsorption system for removal of contaminants and the selection of the appropriate adsorbent.

4.7.1. Langmuir adsorption isotherm model

The experimental data were analyzed according to the linear form of the Langmuir isotherm as described in equation 4. Figure 21 showed the experimental results obtained from the Langmuir isotherm experiment. As presented in Table 5, the correlation coefficient value (R^2 = 0.9808) indicates that the Langmuir model adequately fits to describe the equilibrium adsorption of MB onto AC-Fe_3O_4 composite adsorbent. The well-fitting of the Langmuir model also shows the presence of monolayer MB coverage on the homogeneous active sites of AC-Fe_3O_4 composite adsorbent which is consistent with the pseudo-second-order model interpretation. The Langmuir model can also be used to determine the feasibility of MB

adsorption onto AC-Fe_3O_4 composite adsorbent based on the R_L value which is dimensionless constant expressed in eq (5). The R_L value for the AC-Fe_3O_4 composite adsorbent in this study is 0.056, implying favorable adsorption for MB from aqueous solution (Gao et al., 2013, Ajmal et al., 2018; Abebe et al., 2018). The maximum MB adsorption capacity of the AC-Fe_3O_4 composite adsorbent determined from the Langmuir isotherm model was found to be 47.39 mg/ g.

Table 5: Summary of adsorption isotherm parameters using Langmuir isotherm model.

Pollutant	Co(mg/L)	q_e(mg/g)	Intercept	Slope	q_m(mg/g)	R_L	R^2
MB	50	36.04	0.0629	0.0211	47.39	0.056	0.9807

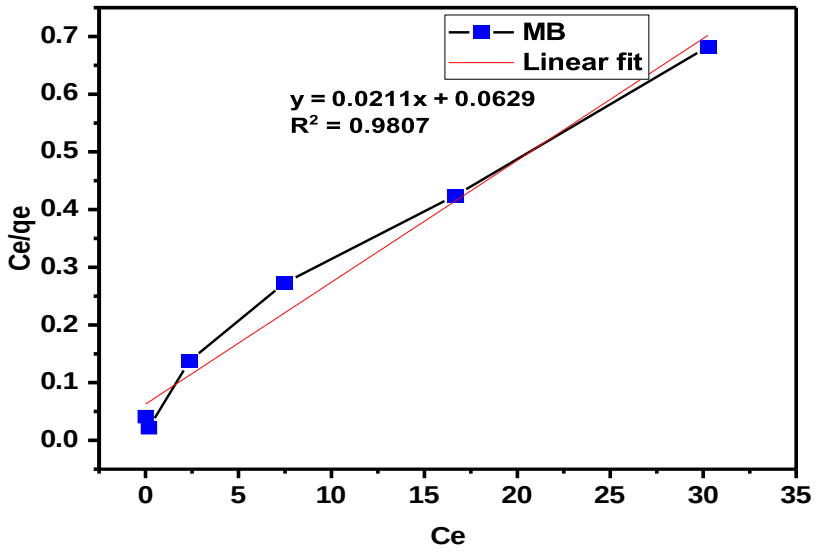

Figure 19**:** Langmuir adsorption isotherm model.

4.7.2. Freundlich adsorption isotherm model

The Freundlich isotherm model was the second model used to describe the adsorption data of MB in which the Freundlich constant K_F (mg/g), and n is characteristic constants related to the relative adsorption capacity of the adsorbent and the intensity of adsorption, respectively. The K_F and 1/n can be obtained from the intercept and slope of the linear plot of Logqe versus LogCe. The Freundlich plots between Logqe versus LogCe for the adsorption of MB are shown in Figure 22.The applicability of the Freundlich adsorption isotherm was also analyzed, using the same set of experimental data as for the Langmuir model. Thus, from

Table 6, the Langmuir isotherm model exhibited a better mathematical fit to experimental data (R^2 = 0.9719) than the Freundlich isotherm model (R^2 = 0.9100), suggesting that the adsorption of the MB onto AC-Fe_3O_4 composite adsorbent could be favorably described by the Langmuir isotherm model. It is clear that the equilibrium adsorption data comply with Langmuir isotherm model, which suggests that the adsorption is a process which occurs in a homogeneous surface. Additionally, these results also demonstrated no interaction and transmigration of dyes in the plane of the neighboring surface (Foo et al., 2011).

Table 6: Summary of adsorption isotherm parameters using Freundlich isotherm model.

Pollutant	Co(mg/L)	Intercept	Slope	1/n	KF	R^2
MB	50	-1.2842	1.4525	0.55	7.511	0.9100

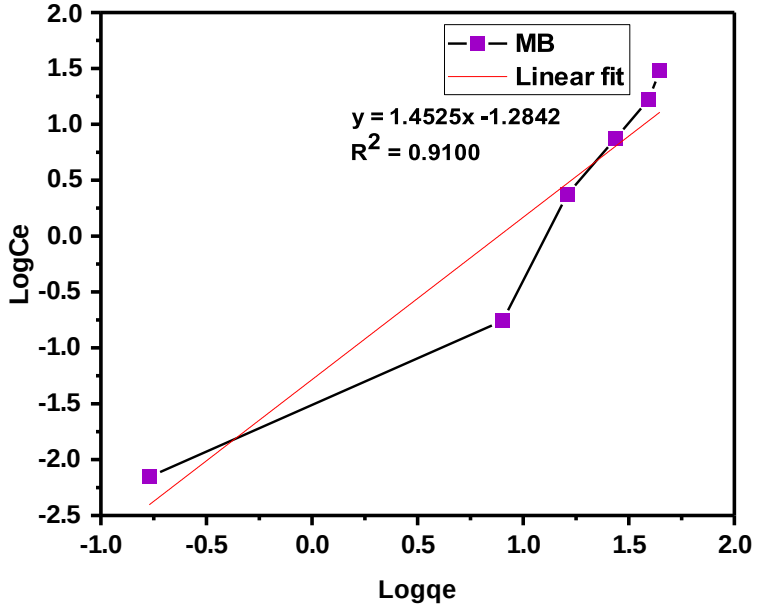

Figure 20**:** Freundlich adsorption isotherm model

4.8. Recyclability of AC-Fe_3O_4 Adsorbent

Due to its magnetic property, the synthesized nanocomposite can be used for several times by separating the used adsorbent using external magnet and washing it by deionized water. Re-usability of the AC-Fe_3O_4 composite adsorbent was assessed for six consecutive MB adsorption cycles. The desorption process for the MB previously adsorbed on the AC-Fe_3O_4 composite adsorbent was optimized to be able to reuse the nanoadsorbents for further adsorption process and to recover the AC-Fe_3O_4. The average desorption efficiency of the adsorbent was found to be about 85.17% which indicates that the adsorption of MB on the

adsorbent involves physical in addition to chemical adsorption process. Figure 23 and Table7 showed the removal efficiency for each cycle for AC-Fe_3O_4 nanocomposite adsorbent using the desorption solution. There was a gradual decrease in MB removal efficiencies with an increasing number of cycles as shown in Figure 23. The removal efficiencies of MB for 1, 2, 3, 4, 5, and 6 cycles were found to be 98.10%, 95.93, 91.24%, 88.71%, 86.55%, and 82.86% respectively. Hence, the MB uptake capacity on the AC-Fe_3O_4 nanocomposite adsorbent was reduced as the number of cycles increase. The regeneration experiments presented in Figure 23 showed that the AC-Fe_3O_4 nanocomposite adsorbent could be reused repeatedly in the adsorption and removal of MB without significantly losing the adsorption property. Similar results were reported by different studies (Y. Zhang et al., 2020; B. Wu et al., 2017).

Table 7: Recyclability of AC-Fe_3O_4 nanocomposite adsorbent for MB removal

Cycle	Co(mg/L)	Ce(mg/L)	% Removal
1	50	0.105	98.10
2	50	2.035	95.93
3	50	3.381	91.24
4	50	5.643	88.71
5	50	6.725	86.55
6	50	8.570	82.86

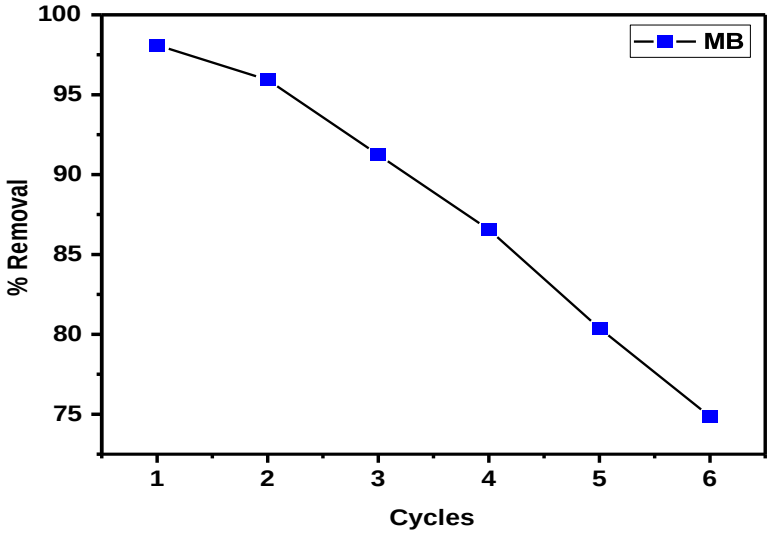

Figure 21**:** Recyclability test of AC-Fe_3O_4 nanocomposite adsorbent for MB removal.

5. CONCLUSION AND RECOMMENDATION

5.1. Conclusions

This study examined the removal of MB from wastewater by using a low-cost adsorbent, AC-Fe_3O_4 nanocomposite. The different physicochemical and surface characteristics of the AC pyrolyzed at temperatures of 450 °C, 550 °C and 650 °C and labeled (AC450, AC550, and AC650) confirmed the AC550 has better potential for MB dye decontamination. Moreover, the different surface characteristics of AC, Fe_3O_4 as well as AC-Fe_3O_4 nanocomposite adsorbent revealed the presence of suitable functional groups for MB adsorption like (-OH), (C-N), (C-O), and (Fe-O), rough structure, and highly porous surface characteristics that influence its adsorption efficiency.

Adsorption parameters such as solution pH, contact time, initial concentration of MB and adsorbent dose significantly influence the removal efficiency of the composite adsorbent and needs to be optimized for its effective use. The AC-Fe_3O_4 nanocomposite adsorbent has maximum adsorption capacity of 49.94 mg/g with removal efficiency of 99.98 % at optimized contact time of 15 minutes, initial MB dye concentration of 50 mg/L, and 0.1g of AC-Fe_3O_4 nanocomposite dose at room temperature with stirring rate of 150 rpm.

The adsorption process of this study was well described by the Langmuir model with a high R^2 value of 0.9807 than Freundlich model, which indicated the adsorption mechanism is monolayer adsorption processes and the presence of homogenous sites on the AC-Fe_3O_4 nanocomposite surface. The data from kinetic experiments was found to fit well with the pseudo-second-order kinetic model with a high R^2 value of 0.9989, which indicates the presence of chemisorption.

AC-Fe_3O_4 nanocomposite also exhibited good magnetic property for easy recovery, excellent recyclability and environmental friendliness. Further, MB adsorbed onto the AC-Fe_3O_4 nanocomposite was eluted by using hydrochloric acid solution. The nanocomposite has shown excellent reusability for six consecutive adsorption-desorption cycles. The reusability study has shown that the synthesized AC-Fe_3O_4 nano composite adsorbent material has a very good potential applicability to remove MB from wastewater effluent.

5.2. Recommendation

Because of its simplicity and low cost, it is better for researcher to further studies on AC-Fe_3O_4 composite for MB removal from wastewaters. It is also possible to study the efficiency of the desorption process by using different eluent to get a full picture of the removal capacity of the AC-Fe_3O_4 composite for MB and other pollutants removal from different types of wastewater. The multifunctional properties of the AC-Fe_3O_4 composite beyond adsorption of MB should be investigated like metal ions removal from seawater and humic substances, naturally occurring organic polymeric compounds widely distributed in wastewater. The Transmission electron microscopy (TEM) and Brunauer-Emmett-Teller (BET) characterization technique of the AC-Fe_3O_4 composite should be included to determine the particle size, surface area shape and distribution.

Therefore, we recommended that for a researcher it is better to assess by expanding this study to obtain new AC-Fe_3O_4 composite with enhanced MB adsorption, heavy metals removal capabilities over a wider pH range, easy synthesis method and separation techniques to overcome these disadvantages.

6. REFERENCE

. M., Shukla, S. P., & Mohan, D. (2017). Toxicity of Disperse Dyes and its Removal from Wastewater Using Various Adsorbents: A Review. *Research Journal of Environmental Toxicology*, *11*(2), 72–89. https://doi.org/10.3923/rjet.2017.72.89

Abebe, B., Murthy, H. C. A., & Faga, M. G. (2018). Synthesis and Characterization of Ti-Fe Oxide Nanomaterials for Lead Removal. *Journal of Nanomaterials*, *2018*. https://doi.org/10.1155/2018/9651039

Adegoke, K. A., & Bello, O. S. (2015). Dye sequestration using agricultural wastes as adsorbents. *Water Resources and Industry*, *12*, 8–24. https://doi.org/10.1016/j.wri.2015.09.002

Adiba, Pandey, V., Munjal, S., & Ahmad, T. (2019). Structural, morphological and magnetic properties of antiferromagnetic nickel oxide nanoparticles synthesized via sol-gel route. *Materials Today: Proceedings*, *26*(xxxx), 3116–3118. https://doi.org/10.1016/j.matpr.2020.02.643

Aghazadeh, M., Golikand, A. N., Ghaemi, M., & Yousefi, T. (2011). A novel lanthanum hydroxide nanostructure prepared by cathodic electrodeposition. *Materials Letters*, *65*(10), 1466–1468. https://doi.org/10.1016/j.matlet.2011.02.039

Ahmad, A., Mohd-setapar, S. H., Chuong, S., & Khatoon, A. (2015). *RSC Advances Recent advances in new generation dye removal technologies : novel search for approaches to reprocess wastewater*. 30801–30818. https://doi.org/10.1039/c4ra16959j

Ahmad, T., Pandey, V., Husain, M. S., Adiba, & Munjal, S. (2021). Structural and spectroscopic analysis of pure phase hexagonal wurtzite ZnO nanoparticles synthesized by sol-gel. *Materials Today: Proceedings*, *49*(xxxx), 1694–1697. https://doi.org/10.1016/j.matpr.2021.07.456

Ahmed, S., Ashiq, M. N., Li, D., Tang, P., Leroux, F., & Feng, Y. (2019). Recent Progress on Adsorption Materials for Phosphate Removal. *Recent Patents on Nanotechnology*, *13*(1), 3–16. https://doi.org/10.2174/1872210513666190306155245

Ajinkya, N., Yu, X., Kaithal, P., Luo, H., & Somani, P. (2020). *Magnetic Iron Oxide Nanoparticle (IONP) Synthesis to Applications : Present and Future*. 1–35.

Ajmal, Z., Muhmood, A., Usman, M., Kizito, S., Lu, J., Dong, R., & Wu, S. (2018). Phosphate removal from aqueous solution using iron oxides : adsorption , desorption and regeneration characteristics. *Journal of Colloid And Interface Science*. https://doi.org/10.1016/j.jcis.2018.05.084

Aljeboree, A. M., Alshirifi, A. N., & Alkaim, A. F. (2017). Kinetics and equilibrium study for the adsorption of textile dyes on coconut shell activated carbon. *Arabian Journal of Chemistry*, *10*, S3381–S3393. https://doi.org/10.1016/j.arabjc.2014.01.020

Anastopoulos, I., & Kyzas, G. Z. (2014). Agricultural peels for dye adsorption: A review of recent literature. *Journal of Molecular Liquids*, *200*(PB), 381–389. https://doi.org/10.1016/j.molliq.2014.11.006

Angin, D. (2014). Utilization of activated carbon produced from fruit juice industry solid waste for the adsorption of Yellow 18 from aqueous solutions. *Bioresource Technology*, *168*, 259–266. https://doi.org/10.1016/j.biortech.2014.02.100

Aragaw, S. G. (2020). *Degradation of Methyl Orange by Fenton Reaction using CuAl-layered double hydroxide / MgO 2 Composite Catalyst under Dark Condition Degradation of Methyl Orange by Fenton Reaction using CuAl- LDH / MgO 2 Composite Catalyst under Dark Condition*.

Ataei-Germi, T., & Nematollahzadeh, A. (2016). Bimodal porous silica microspheres decorated with polydopamine nano-particles for the adsorption of methylene blue in fixed-bed columns. *Journal of Colloid and Interface Science*, *470*, 172–182. https://doi.org/10.1016/j.jcis.2016.02.057

Ayawei, N., Ebelegi, A. N., & Wankasi, D. (2017). Modelling and Interpretation of Adsorption Isotherms. *Journal of Chemistry*, *2017*. https://doi.org/10.1155/2017/3039817

Bagheri, A. R., Ghaedi, M., Asfaram, A., Bazrafshan, A. A., & Jannesar, R. (2017). Comparative study on ultrasonic assisted adsorption of dyes from single system onto Fe3O4 magnetite nanoparticles loaded on activated carbon: Experimental design methodology. *Ultrasonics Sonochemistry*, *34*, 294–304. https://doi.org/10.1016/j.ultsonch.2016.05.047

Batool, F., Akbar, J., Iqbal, S., Noreen, S., & Bukhari, S. N. A. (2018). Study of Isothermal, Kinetic, and Thermodynamic Parameters for Adsorption of Cadmium: An Overview of Linear and Nonlinear Approach and Error Analysis. *Bioinorganic Chemistry and Applications*, *2018*. https://doi.org/10.1155/2018/3463724

Begum, R., Farooqi, Z. H., Naseem, K., Ali, F., Batool, M., Xiao, J., & Irfan, A. (2018). Applications of UV/Vis Spectroscopy in Characterization and Catalytic Activity of Noble Metal Nanoparticles Fabricated in Responsive Polymer Microgels: A Review. *Critical Reviews in Analytical Chemistry*, *48*(6), 503–516. https://doi.org/10.1080/10408347.2018.1451299

Begum, R., Najeeb, J., Sattar, A., Naseem, K., & Irfan, A. (2019). *Chemical reduction of methylene blue in the presence of nanocatalysts : a critical review.*

Bhatnagar, A., & Sillanpää, M. (2010). Utilization of agro-industrial and municipal waste materials as potential adsorbents for water treatment-A review. *Chemical Engineering Journal*, *157*(2–3), 277–296. https://doi.org/10.1016/j.cej.2010.01.007

Bhatnagar, A., Sillanpää, M., & Witek-Krowiak, A. (2015). Agricultural waste peels as versatile biomass for water purification - A review. *Chemical Engineering Journal*, *270*, 244–271. https://doi.org/10.1016/j.cej.2015.01.135

Bilgiç, A., & Çimen, A. (2019). Removal of chromium(vi) from polluted wastewater by chemical modification of silica gel with 4-acetyl-3-hydroxyaniline. *RSC Advances*, *9*(64), 37403–37414. https://doi.org/10.1039/c9ra05810a

Boonamnuayvitaya, V., Sae-Ung, S., & Tanthapanichakoon, W. (2005). Preparation of activated carbons from coffee residue for the adsorption of formaldehyde. *Separation and Purification Technology*, *42*(2), 159–168. https://doi.org/10.1016/j.seppur.2004.07.007

Buketov, A. V., Sapronov, O. O., & Brailo, M. V. (2014). Investigation of the Physico-Mechanical and Thermophysical Properties of Epoxy Composites with a Two-Component Bidisperse Filler. *Strength of Materials*, *46*(5), 717–723. https://doi.org/10.1007/s11223-014-9605-z

Bulgariu, L., Escudero, L. B., Bello, O. S., Iqbal, M., Nisar, J., Adegoke, K. A., Alakhras, F., Kornaros, M., & Anastopoulos, I. (2019). The utilization of leaf-based adsorbents for dyes removal: A review. *Journal of Molecular Liquids*, *276*, 728–747.

https://doi.org/10.1016/j.molliq.2018.12.001

Cazetta, A. L., Pezoti, O., Bedin, K. C., Silva, T. L., Paesano Junior, A., Asefa, T., & Almeida, V. C. (2016). Magnetic Activated Carbon Derived from Biomass Waste by Concurrent Synthesis: Efficient Adsorbent for Toxic Dyes. *ACS Sustainable Chemistry and Engineering*, *4*(3), 1058–1068. https://doi.org/10.1021/acssuschemeng.5b01141

Chaudhary, R., Nawaz, K., Khan, A. K., Hano, C., Abbasi, B. H., & Anjum, S. (2020). An overview of the algae-mediated biosynthesis of nanoparticles and their biomedical applications. *Biomolecules*, *10*(11), 1–35. https://doi.org/10.3390/biom10111498

Chen, B., Chen, Z., & Lv, S. (2011). A novel magnetic biochar efficiently sorbs organic pollutants and phosphate. *Bioresource Technology*, *102*(2), 716–723. https://doi.org/10.1016/j.biortech.2010.08.067

Chen, Y., Xu, R., Li, Y., Liu, Y., Wu, Y., Chen, Y., Zhang, J., Chen, S., Yin, H., Zeng, Z., Wang, S., & Peng, Z. (2020). La(OH)3-modified magnetic CoFe2O4 nanocomposites: A novel adsorbent with highly efficient activity and reusability for phosphate removal. *Colloids and Surfaces A: Physicochemical and Engineering Aspects*, *599*(May), 1–11. https://doi.org/10.1016/j.colsurfa.2020.124870

Cheng, W., Zhang, W., Hu, L., Ding, W., Wu, F., & Li, J. (2016). Etching synthesis of iron oxide nanoparticles for adsorption of arsenic from water. *RSC Advances*, *6*(19), 15900–15910. https://doi.org/10.1039/c5ra26143k

Coates, J. (2006). Interpretation of Infrared Spectra, A Practical Approach. *Encyclopedia of Analytical Chemistry*, 1–23. https://doi.org/10.1002/9780470027318.a5606

Contescu, C., Adhikari, S., Gallego, N., Evans, N., & Biss, B. (2018). Activated Carbons Derived from High-Temperature Pyrolysis of Lignocellulosic Biomass. *C*, *4*(3), 51. https://doi.org/10.3390/c4030051

Crini, G., & Badot, P. M. (2008). Application of chitosan, a natural aminopolysaccharide, for dye removal from aqueous solutions by adsorption processes using batch studies: A review of recent literature. *Progress in Polymer Science (Oxford)*, *33*(4), 399–447. https://doi.org/10.1016/j.progpolymsci.2007.11.001

Crini, G., Lichtfouse, E., Wilson, L. D., & Morin-Crini, N. (2019). Conventional and non-conventional adsorbents for wastewater treatment. *Environmental Chemistry Letters*, *17*(1), 195–213. https://doi.org/10.1007/s10311-018-0786-8

Daneshvar Tarigh, G., & Shemirani, F. (2013). Magnetic multi-wall carbon nanotube nanocomposite as an adsorbent for preconcentration and determination of lead (II) and manganese (II) in various matrices. *Talanta*, *115*, 744–750. https://doi.org/10.1016/j.talanta.2013.06.018

Daud, M. K., Nafees, M., Ali, S., Rizwan, M., Bajwa, R. A., Shakoor, M. B., Arshad, M. U., Chatha, S. A. S., Deeba, F., Murad, W., Malook, I., & Zhu, S. J. (2017). Drinking Water Quality Status and Contamination in Pakistan. *BioMed Research International*, *2017*. https://doi.org/10.1155/2017/7908183

Deliyanni, E. A., Peleka, E. N., & Lazaridis, N. K. (2007). Comparative study of phosphates removal from aqueous solutions by nanocrystalline akaganéite and hybrid surfactant-akaganéite. *Separation and Purification Technology*, *52*(3), 478–486. https://doi.org/10.1016/j.seppur.2006.05.028

Demirbas, A. (2009). *Agricultural based activated carbons for the removal of dyes from aqueous solutions : A review*. *167*, 1–9. https://doi.org/10.1016/j.jhazmat.2008.12.114

Desore, A., & Narula, S. A. (2018). An overview on corporate response towards sustainability issues in textile industry. *Environment, Development and Sustainability*, *20*(4), 1439–1459. https://doi.org/10.1007/s10668-017-9949-1

Devi, P., & Saroha, A. K. (2017). Utilization of sludge based adsorbents for the removal of various pollutants: A review. *Science of the Total Environment*, *578*, 16–33. https://doi.org/10.1016/j.scitotenv.2016.10.220

Din, S. H. (2019). Nano-Composites and their Applications: A review. *Characterization and Application of Nanomaterials*, *2*(1), 1–9. https://doi.org/10.24294/can.v2i1.875

El-sayed, M. E. A. (2020a). Jo ur l P of. *Science of the Total Environment*, 139903. https://doi.org/10.1016/j.scitotenv.2020.139903

El-sayed, M. E. A. (2020b). Nanoadsorbents for water and wastewater remediation. *Science of the Total Environment*, *739*, 139903. https://doi.org/10.1016/j.scitotenv.2020.139903

El-Tokhy, T., Ahmed, M., ElGamma, M., & Ibrahim, M. (2020). Improvement and characterization of alum sludge by nano-iron oxide and rice husk for removal of methylene blue dye from aqueous solution. *Journal of Egyptian Academic Society for Environmental Development. D, Environmental Studies*, *21*(1), 25–59. https://doi.org/10.21608/jades.2020.145445

Elwakeel, K. Z., Elgarahy, A. M., Khan, Z. A., Almughamisi, M. S., & Al-Bogami, A. S. (2020). Perspectives regarding metal/mineral-incorporating materials for water purification: With special focus on Cr(vi) removal. *Materials Advances*, *1*(6), 1546–1574. https://doi.org/10.1039/d0ma00153h

Fan, S., Wang, Y., Wang, Z., Tang, J., Tang, J., & Li, X. (2017). Removal of methylene blue from aqueous solution by sewage sludge-derived biochar: Adsorption kinetics, equilibrium, thermodynamics and mechanism. *Journal of Environmental Chemical Engineering*, *5*(1), 601–611. https://doi.org/10.1016/j.jece.2016.12.019

Ferreira, R. T. L., Amatte, I. C., Dutra, T. A., & Bürger, D. (2017). Experimental characterization and micrography of 3D printed PLA and PLA reinforced with short carbon fibers. *Composites Part B: Engineering*, *124*, 88–100. https://doi.org/10.1016/j.compositesb.2017.05.013

Foo, K. Y., & Hameed, B. H. (2011). Preparation and characterization of activated carbon from sunflower seed oil residue via microwave assisted K 2CO 3 activation. *Bioresource Technology*, *102*(20), 9794–9799. https://doi.org/10.1016/j.biortech.2011.08.007

Fu, H., Yang, Y., Zhu, R., Liu, J., Usman, M., Chen, Q., & He, H. (2018). Superior adsorption of phosphate by ferrihydrite-coated and lanthanum-decorated magnetite. *Journal of Colloid and Interface Science*, *530*, 704–713. https://doi.org/10.1016/j.jcis.2018.07.025

Gao, J., Qin, Y., Zhou, T., & Cao, D. (2013). *Adsorption of methylene blue onto activated carbon produced from tea (Camellia sinensis L .) seed shells : kinetics , equilibrium , and thermodynamics studies *. 14*(7), 650–658. https://doi.org/10.1631/jzus.B12a0225

Georgin, J., Yamil, Y. L., Franco, D. S. P., Netto, M. S., Piccilli, D. G. A., Perondi, D., Silva, L. F. O., Foletto, E. L., & Dotto, G. L. (2021). Development of highly porous activated carbon from Jacaranda mimosifolia seed pods for remarkable removal of aqueous-phase ketoprofen. *Journal of Environmental Chemical Engineering*, *9*(4). https://doi.org/10.1016/j.jece.2021.105676

Gong, J. L., Wang, B., Zeng, G. M., Yang, C. P., Niu, C. G., Niu, Q. Y., Zhou, W. J., & Liang, Y. (2009). Removal of cationic dyes from aqueous solution using magnetic multi-wall carbon nanotube nanocomposite as adsorbent. *Journal of Hazardous Materials*, *164*(2–3), 1517–1522. https://doi.org/10.1016/j.jhazmat.2008.09.072

Gunarathne, V., Ashiq, A., & Ginige, M. P. (2018). *Green Adsorbents for Pollutant Removal*. *18*. https://doi.org/10.1007/978-3-319-92111-2

Guo, K., Gao, B., Li, R., Wang, W., Yue, Q., & Wang, Y. (2018). Flocculation performance of lignin-based flocculant during reactive blue dye removal: comparison with commercial flocculants. *Environmental Science and Pollution Research*, *25*(3), 2083–2095. https://doi.org/10.1007/s11356-017-0835-z

Hassaan, M., & Nemr, A. el. (2017). Health and Environmental Impacts of Dyes: Mini Review. *American Journal of Environmental Science and Engineering*, *1*(3), 64–67. https://doi.org/10.11648/j.ajese.20170103.11

Ho, Y. S., Chiang, T. H., & Hsueh, Y. M. (2005). Removal of basic dye from aqueous solution using tree fern as a biosorbent. *Process Biochemistry*, *40*(1), 119–124. https://doi.org/10.1016/j.procbio.2003.11.035

Hu, Q., & Zhang, Z. (2019). Application of Dubinin–Radushkevich isotherm model at the solid/solution interface: A theoretical analysis. *Journal of Molecular Liquids*, *277*, 646–648. https://doi.org/10.1016/j.molliq.2019.01.005

Huang, W. Y., Li, D., Liu, Z. Q., Tao, Q., Zhu, Y., Yang, J., & Zhang, Y. M. (2014). Kinetics, isotherm, thermodynamic, and adsorption mechanism studies of La(OH)3-modified exfoliated vermiculites as highly efficient phosphate adsorbents. *Chemical Engineering Journal*, *236*, 191–201. https://doi.org/10.1016/j.cej.2013.09.077

Ijaz, I., Gilani, E., Nazir, A., & Bukhari, A. (2020). Detail review on chemical, physical and green synthesis, classification, characterizations and applications of nanoparticles. *Green Chemistry Letters and Reviews*, *13*(3), 59–81. https://doi.org/10.1080/17518253.2020.1802517

Ismail, L., Khalili, F., & Abu Orabi, F. M. (2020). Modification of Silica Nanoparticles with Cysteine or Methionine Amino Acids for the Removal of Uranium (VI) from Aqueous Solution. *Silicon*, *12*(11), 2647–2661. https://doi.org/10.1007/s12633-019-00361-9

Jiang, W., Tao, T., & Liao, Z.-M. (2011). Removal of Heavy Metal from Contaminated Soil with Chelating Agents. *Open Journal of Soil Science*, *01*(02), 70–76. https://doi.org/10.4236/ojss.2011.12010

Joshi, S., Sharma, M., Kumari, A., Shrestha, S., & Shrestha, B. (2019). Arsenic removal fromwater by adsorption onto iron oxide/nano-porous carbon magnetic composite. *Applied Sciences (Switzerland)*, *9*(18). https://doi.org/10.3390/app9183732

Kandisa, R. V., Kv, N. S., Shaik, K. B., & Gopinath, R. (2016). *Bioremediation & Biodegradation Dye Removal by Adsorption : A Review*. *7*(6). https://doi.org/10.4172/2155-6199.1000371

Kara, H. T., Anshebo, S. T., Sabir, F. K., & Workineh, G. A. (2021). *Removal of Methylene Blue Dye from Wastewater Using Periodiated Modified Nanocellulose*. *2021*.

Karaer, H., & Kaya, I. (2016). Synthesis, characterization of magnetic chitosan/active charcoal composite and using at the adsorption of methylene blue and reactive blue4. *Microporous and Mesoporous Materials*, *232*, 26–38. https://doi.org/10.1016/j.micromeso.2016.06.006

Kaur, S., & Kaur, P. (2019). Nanoparticles Characterization and Applications: An Overview. *Indo Global Journal of Pharmaceutical Sciences*, *09*(02), 146–146. https://doi.org/10.35652/igjps.2019.92s44

Khatri, A., Peerzada, M. H., Mohsin, M., & White, M. (2015). A review on developments in dyeing cotton fabrics with reactive dyes for reducing effluent pollution. *Journal of Cleaner Production*, *87*(1), 50–57. https://doi.org/10.1016/j.jclepro.2014.09.017

Koilraj, P., & Sasaki, K. (2017). Selective removal of phosphate using La-porous carbon composites from aqueous solutions: Batch and column studies. *Chemical Engineering Journal*, *317*, 1059–1068. https://doi.org/10.1016/j.cej.2017.02.075

Kumar, L., Alam, M. S., Meena, C. L., Jain, R., & Bansal, A. K. (2009). Chapter 4 Fexofenadine Hydrochloride. In *Profiles of Drug Substances, Excipients and Related Methodology* (1st ed., Vol. 34, Issue 08). Elsevier Inc. https://doi.org/10.1016/S1871-5125(09)34004-2

Kurniawan, T. A., Chan, G. Y. S., Lo, W. H., & Babel, S. (2006). Physico-chemical treatment techniques for wastewater laden with heavy metals. *Chemical Engineering Journal*, *118*(1–2), 83–98. https://doi.org/10.1016/j.cej.2006.01.015

Lai, L., Xie, Q., Chi, L., Gu, W., & Wu, D. (2016). Adsorption of phosphate from water by easily separable Fe3O4@SiO2 core/shell magnetic nanoparticles functionalized with hydrous lanthanum oxide. *Journal of Colloid and Interface Science*, *465*, 76–82.

https://doi.org/10.1016/j.jcis.2015.11.043

Laysandra, L., Sari, M. W. M. K., Soetaredjo, F. E., Foe, K., Putro, J. N., Kurniawan, A., Ju, Y. H., & Ismadji, S. (2017). Adsorption and photocatalytic performance of bentonite-titanium dioxide composites for methylene blue and rhodamine B decoloration. *Heliyon*, *3*(12), e00488. https://doi.org/10.1016/j.heliyon.2017.e00488

Li, X., Deng, S., & Fu, H. (2012). Inhibition of the corrosion of steel in HCl, H 2SO 4 solutions by bamboo leaf extract. *Corrosion Science*, *62*, 163–175. https://doi.org/10.1016/j.corsci.2012.05.008

Lima, A. R. A., Baltazar-soares, M., Garrido, S., Carrera, P., Piecho-santos, A. M., Peck, M. A., & Silva, G. (2021). Jo ur l P of. *Science of the Total Environment*, 150167. https://doi.org/10.1016/j.scitotenv.2021.150167

Limousin, G., Gaudet, J. P., Charlet, L., Szenknect, S., Barthès, V., & Krimissa, M. (2007). Sorption isotherms: A review on physical bases, modeling and measurement. *Applied Geochemistry*, *22*(2), 249–275. https://doi.org/10.1016/j.apgeochem.2006.09.010

Lin, Z., & Chen, J. (2021). Magnetic Fe3O4@MgAl-LDH@La(OH)3 composites with a hierarchical core-shell structure for phosphate removal from wastewater and inhibition of labile sedimentary phosphorus release. *Chemosphere*, *264*, 128551. https://doi.org/10.1016/j.chemosphere.2020.128551

Liou, T. (2010). Development of mesoporous structure and high adsorption capacity of biomass-based activated carbon by phosphoric acid and zinc chloride activation. *Chemical Engineering Journal*, *158*(2), 129–142. https://doi.org/10.1016/j.cej.2009.12.016

Liu, S. J., Li, J., Yang, Y. K., Wang, J., & Ding, H. (2016). Influence of environmental factors on the phosphorus adsorption of lanthanum-modified bentonite in eutrophic water and sediment. *Environmental Science and Pollution Research*, *23*(3), 2487–2494. https://doi.org/10.1007/s11356-015-5453-z

Liu, Xiaoduo, Tian, J., Li, Y., Sun, N., Mi, S., Xie, Y., & Chen, Z. (2019). Enhanced dyes adsorption from wastewater via Fe3O4 nanoparticles functionalized activated carbon. *Journal of Hazardous Materials*, *373*(March), 397–407. https://doi.org/10.1016/j.jhazmat.2019.03.103

Liu, Xiaohuan, Zong, E., Hu, W., Song, P., Wang, J., Liu, Q., Ma, Z., & Fu, S. (2019). Lignin-Derived Porous Carbon Loaded with La(OH) 3 Nanorods for Highly Efficient Removal of Phosphate. *ACS Sustainable Chemistry and Engineering*, *7*(1), 758–768. https://doi.org/10.1021/acssuschemeng.8b04382

Liu, Y. (2008). New insights into pseudo-second-order kinetic equation for adsorption. *Colloids and Surfaces A: Physicochemical and Engineering Aspects*, *320*(1–3), 275–278. https://doi.org/10.1016/j.colsurfa.2008.01.032

Lunge, S., Singh, S., & Sinha, A. (2014). Magnetic iron oxide (Fe3O4) nanoparticles from tea waste for arsenic removal. *Journal of Magnetism and Magnetic Materials*, *356*, 21–31. https://doi.org/10.1016/j.jmmm.2013.12.008

Macys, J. J. (2005). On estimates of factorial quotients. *Lithuanian Mathematical Journal*, *45*(3), 284–291. https://doi.org/10.1007/s10986-005-0030-7

Mani, T., Murugan, P., Abedi, J., & Mahinpey, N. (2010). Pyrolysis of wheat straw in a thermogravimetric analyzer: Effect of particle size and heating rate on devolatilization and estimation of global kinetics. *Chemical Engineering Research and Design*, *88*(8), 952–958. https://doi.org/10.1016/j.cherd.2010.02.008

Mazloumi, M., Shahcheraghi, N., Kajbafvala, A., Zanganeh, S., Lak, A., Mohajerani, M. S., & Sadrnezhaad, S. K. (2009). 3D bundles of self-assembled lanthanum hydroxide nanorods via a rapid microwave-assisted route. *Journal of Alloys and Compounds*, *473*(1–2), 283–287. https://doi.org/10.1016/j.jallcom.2008.05.052

Menya, E., Olupot, P. W., Storz, H., Lubwama, M., & Kiros, Y. (2018). Production and performance of activated carbon from rice husks for removal of natural organic matter from water: A review. *Chemical Engineering Research and Design*, *129*, 271–296. https://doi.org/10.1016/j.cherd.2017.11.008

Miraboutalebi, S. M., Nikouzad, S. K., Peydayesh, M., Allahgholi, N., Vafajoo, L., & McKay, G. (2017). Methylene blue adsorption via maize silk powder: Kinetic, equilibrium, thermodynamic studies and residual error analysis. *Process Safety and Environmental Protection*, *106*, 191–202. https://doi.org/10.1016/j.psep.2017.01.010

Mironyuk, I., Tatarchuk, T., Naushad, M., Vasylyeva, H., & Mykytyn, I. (2019). Highly efficient adsorption of strontium ions by carbonated mesoporous TiO 2. *Journal of Molecular Liquids*, *285*, 742–753. https://doi.org/10.1016/j.molliq.2019.04.111

Mohammad Mostafa. (2015). Waste water treatment in Textile Industries- the concept and current removal Waste water treatment in textile Industries - the concept and current removal technologies Mohammad Mostafa. *Journal of Biodiversity and Environmental Sciences (JBES)*, *7*(May), 501–525.

Mohammed, M. A., Shitu, A., & Ibrahim, A. (2014). *Removal of Methylene Blue Using Low Cost Adsorbent : A Review Removal of Methylene Blue Using Low Cost Adsorbent : A Review*. *November*.

Mohapatra, M., & Anand, S. (2011). Synthesis and applications of nano-structured iron oxides/hydroxides – a review. *International Journal of Engineering, Science and Technology*, *2*(8), 127–146. https://doi.org/10.4314/ijest.v2i8.63846

Mohd Udaiyappan, A. F., Abu Hasan, H., Takriff, M. S., & Sheikh Abdullah, S. R. (2017). A review of the potentials, challenges and current status of microalgae biomass applications in industrial wastewater treatment. *Journal of Water Process Engineering*, *20*(June), 8–21. https://doi.org/10.1016/j.jwpe.2017.09.006

Monama, G. R., Mdluli, S. B., Mashao, G., Makhafola, M. D., Ramohlola, K. E., Molapo, K. M., Hato, M. J., Makgopa, K., Iwuoha, E. I., & Modibane, K. D. (2018). Palladium deposition on copper(II) phthalocyanine/metal organic framework composite and electrocatalytic activity of the modified electrode towards the hydrogen evolution reaction. *Renewable Energy*, *119*, 62–72. https://doi.org/10.1016/j.renene.2017.11.084

Moosavi, S., Lai, C. W., Gan, S., Zamiri, G., Akbarzadeh Pivehzhani, O., & Johan, M. R. (2020). Application of efficient magnetic particles and activated carbon for dye removal from wastewater. *ACS Omega*, *5*(33), 20684–20697. https://doi.org/10.1021/acsomega.0c01905

Mourdikoudis, S., Pallares, R. M., & Thanh, N. T. K. (2018). Characterization techniques for nanoparticles: Comparison and complementarity upon studying nanoparticle properties. *Nanoscale*, *10*(27), 12871–12934. https://doi.org/10.1039/c8nr02278j

Muniz, F. T. L., Miranda, M. A. R., Morilla Dos Santos, C., & Sasaki, J. M. (2016). The Scherrer equation and the dynamical theory of X-ray diffraction. *Acta Crystallographica Section A: Foundations and Advances*, *72*(3), 385–390. https://doi.org/10.1107/S205327331600365X

Musa, M., Wan Ibrahim, W. A., Mohd Marsin, F., Abdul Keyon, A. S., & Rashidi Nodeh, H. (2018). Graphene-magnetite as adsorbent for magnetic solid phase extraction of 4-hydroxybenzoic acid and 3,4-dihydroxybenzoic acid in stingless bee honey. *Food Chemistry*, *265*(April), 165–172. https://doi.org/10.1016/j.foodchem.2018.04.020

Nanda, S., Mohanty, P., Pant, K. K., Naik, S., Kozinski, J. A., & Dalai, A. K. (2013). Characterization of North American Lignocellulosic Biomass and Biochars in Terms of their Candidacy for Alternate Renewable Fuels. *Bioenergy Research*, *6*(2), 663–677. https://doi.org/10.1007/s12155-012-9281-4

Naz, R., Roberts, T. H., Bano, A., Nosheen, A., Yasmin, H., Hassan, M. N., Keyani, R., Ullah, S., Khan, W., & Anwar, Z. (2020). GC-MS analysis, antimicrobial, antioxidant, antilipoxygenase and cytotoxic activities of Jacaranda mimosifolia methanol leaf extracts and fractions. *PLoS ONE*, *15*(7 July), 1–24. https://doi.org/10.1371/journal.pone.0236319

Pathania, D., Sharma, S., & Singh, P. (2017). Removal of methylene blue by adsorption onto activated carbon developed from Ficus carica bast. *Arabian Journal of Chemistry*, *10*, S1445–S1451. https://doi.org/10.1016/j.arabjc.2013.04.021

Patra, J. K., Ali, M. S., Oh, I. G., & Baek, K. H. (2017). Proteasome inhibitory, antioxidant, and synergistic antibacterial and anticandidal activity of green biosynthesized magnetic Fe3O4 nanoparticles using the aqueous extract of corn (Zea mays L.) ear leaves. *Artificial Cells, Nanomedicine and Biotechnology*, *45*(2), 349–356. https://doi.org/10.3109/21691401.2016.1153484

Qiu, H., Lv, L., Pan, B. C., Zhang, Q. J., Zhang, W. M., & Zhang, Q. X. (2009). Critical review in adsorption kinetic models. *Journal of Zhejiang University: Science A*, *10*(5), 716–724. https://doi.org/10.1631/jzus.A0820524

Qiu, Y., Zheng, Z., Zhou, Z., & Sheng, G. D. (2009). Effectiveness and mechanisms of dye adsorption on a straw-based biochar. *Bioresource Technology*, *100*(21), 5348–5351. https://doi.org/10.1016/j.biortech.2009.05.054

Quist-Jensen, C. A., Macedonio, F., & Drioli, E. (2015). Membrane technology for water production in agriculture: Desalination and wastewater reuse. *Desalination*, *364*, 17–32. https://doi.org/10.1016/j.desal.2015.03.001

Rahimian, R., & Zarinabadi, S. (2020). *A review of Studies on the Removal of Methylene Blue Dye from Industrial Wastewater Using Activated Carbon Adsorbents Made from Almond Bark*. *3*(3), 251–268.

Rahman, M. A., Amin, S. M. R., & Alam, A. M. S. (2012). Removal of Methylene Blue from Waste Water Using Activated Carbon Prepared from Rice Husk. *Dhaka University Journal of Science*, *60*(2), 185–189. https://doi.org/10.3329/dujs.v60i2.11491

Raj, K. G., & Joy, P. A. (2015). Coconut shell based activated carbon-iron oxide magnetic nanocomposite for fast and efficient removal of oil spills. *Journal of Environmental Chemical Engineering*, *3*(3), 2068–2075. https://doi.org/10.1016/j.jece.2015.04.028

Rajbhandari, R., Shrestha, L. K., & Pradhananga, R. R. (1970). Preparation of Activated Carbon from Lapsi Seed Stone and its Application for the Removal of Arsenic from Water. *Journal of the Institute of Engineering*, *8*(1–2), 211–218. https://doi.org/10.3126/jie.v8i1-2.5113

Ramos Filho, F. G., Mélo, T. J. A., Rabello, M. S., & Silva, S. M. L. (2005). Thermal stability of nanocomposites based on polypropylene and bentonite. *Polymer Degradation and Stability*, *89*(3), 383–392. https://doi.org/10.1016/j.polymdegradstab.2004.12.011

Raposo, F., De La Rubia, M. A., & Borja, R. (2009). Methylene blue number as useful indicator to evaluate the adsorptive capacity of granular activated carbon in batch mode: Influence of adsorbate/adsorbent mass ratio and particle size. *Journal of Hazardous Materials*, *165*(1–3), 291–299. https://doi.org/10.1016/j.jhazmat.2008.09.106

Rashed, M. N. (2013). *Adsorption Technique for the Removal of Organic Pollutants from Water and Wastewater*.

Rashid, R., Shafiq, I., Akhter, P., Iqbal, M. J., & Hussain, M. (2021). A state-of-the-art review on wastewater treatment techniques: the effectiveness of adsorption method. *Environmental Science and Pollution Research*, *28*(8), 9050–9066. https://doi.org/10.1007/s11356-021-12395-x

Ravichandran, K., Praseetha, P. K., Arun, T., & Gobalakrishnan, S. (2018). Synthesis of Nanocomposites. In *Synthesis of Inorganic Nanomaterials: Advances and Key Technologies*. Elsevier Ltd. https://doi.org/10.1016/B978-0-08-101975-7.00006-3

Reddy, P. M. K., Verma, P., & Subrahmanyam, C. (2016). Bio-waste derived adsorbent material for methylene blue adsorption. *Journal of the Taiwan Institute of Chemical Engineers*, *58*, 500–508. https://doi.org/10.1016/j.jtice.2015.07.006

Ren, L., Zhang, J., Li, Y., & Zhang, C. (2011). Preparation and evaluation of cattail fiber-based activated carbon for 2,4-dichlorophenol and 2,4,6-trichlorophenol removal. *Chemical Engineering Journal*, *168*(2), 553–561. https://doi.org/10.1016/j.cej.2011.01.021

Rodrigues, L. A., & da Silva, M. L. C. P. (2009). An investigation of phosphate adsorption from aqueous solution onto hydrous niobium oxide prepared by co-precipitation method. *Colloids and Surfaces A: Physicochemical and Engineering Aspects*, *334*(1–3), 191–196. https://doi.org/10.1016/j.colsurfa.2008.10.023

Rodríguez-Reinoso, F., & Molina-Sabio, M. (1992). Activated carbons from lignocellulosic materials by chemical and/or physical activation: an overview. *Carbon*, *30*(7), 1111–1118. https://doi.org/10.1016/0008-6223(92)90143-K

Saadatkhah, N., Carillo Garcia, A., Ackermann, S., Leclerc, P., Latifi, M., Samih, S., Patience, G. S., & Chaouki, J. (2020). Experimental methods in chemical engineering: Thermogravimetric analysis—TGA. *Canadian Journal of Chemical Engineering*, *98*(1), 34–43. https://doi.org/10.1002/cjce.23673

Sánchez-Martín, J., González-Velasco, M., Beltrán-Heredia, J., Gragera-Carvajal, J., & Salguero-Fernández, J. (2010). Novel tannin-based adsorbent in removing cationic dye (Methylene Blue) from aqueous solution. Kinetics and equilibrium studies. *Journal of Hazardous Materials*, *174*(1–3), 9–16. https://doi.org/10.1016/j.jhazmat.2009.09.008

Santoso, E., Ediati, R., Kusumawati, Y., Bahruji, H., Sulistiono, D. O., & Prasetyoko, D. (2020). Review on recent advances of carbon based adsorbent for methylene blue removal from waste water. *Materials Today Chemistry*, *16*, 100233. https://doi.org/10.1016/j.mtchem.2019.100233

Senthil Kumar, P., Vincent, C., Kirthika, K., & Sathish Kumar, K. (2010). Kinetics and equilibrium studies of Pb2+ ion removal from aqueous solutions by use of nano-silversol-coated activated carbon. *Brazilian Journal of Chemical Engineering*, *27*(2), 339–346. https://doi.org/10.1590/s0104-66322010000200012

Serrano, L. S. S. (2014). *Procurement of Activated Carbon from Jacaranda (Mimosifolia).* *3*(2), 5–7.

Sham, A. Y. W., & Notley, S. M. (2018). Adsorption of organic dyes from aqueous solutions using surfactant exfoliated graphene. *Journal of Environmental Chemical Engineering*, *6*(1), 495–504. https://doi.org/10.1016/j.jece.2017.12.028

Sharma, R., Sarswat, A., Pittman, C. U., & Mohan, D. (2017). Cadmium and lead remediation using magnetic and non-magnetic sustainable biosorbents derived from Bauhinia purpurea pods. *RSC Advances*, *7*(14), 8606–8624. https://doi.org/10.1039/C6RA25295H

Simonin, J. P. (2016). On the comparison of pseudo-first order and pseudo-second order rate laws in the modeling of adsorption kinetics. *Chemical Engineering Journal*, *300*, 254–263. https://doi.org/10.1016/j.cej.2016.04.079

Singh, N. B., Nagpal, G., Agrawal, S., & Rachna. (2018). Water purification by using Adsorbents: A Review. *Environmental Technology and Innovation*, *11*, 187–240. https://doi.org/10.1016/j.eti.2018.05.006

Solomon, R. V., Lydia, I. S., Merlin, J. P., & Venuvanalingam, P. (2012). Enhanced photocatalytic degradation of azo dyes using nano Fe 3O 4. *Journal of the Iranian Chemical Society*, *9*(2), 101–109. https://doi.org/10.1007/s13738-011-0033-8

Song, Q., Huang, S., Xu, L., Wang, N., Hu, Z., Luo, X., & Zheng, Z. (2020). Synthesis of magnetite/lanthanum hydroxide composite and magnetite/aluminum hydroxide composite for removal of phosphate. *Science of the Total Environment*, *723*. https://doi.org/10.1016/j.scitotenv.2020.137838

Spessato, L., Bedin, K. C., Cazetta, A. L., Souza, I. P. A. F., Duarte, V. A., Crespo, L. H. S., Silva, M. C., Pontes, R. M., & Almeida, V. C. (2019). KOH-super activated carbon from biomass waste: Insights into the paracetamol adsorption mechanism and thermal regeneration cycles. *Journal of Hazardous Materials*, *371*(February), 499–505. https://doi.org/10.1016/j.jhazmat.2019.02.102

Subramaniam, R., & Kumar Ponnusamy, S. (2015). Novel adsorbent from agricultural waste (cashew NUT shell) for methylene blue dye removal: Optimization by response surface methodology. *Water Resources and Industry*, *11*, 64–70. https://doi.org/10.1016/j.wri.2015.07.002

Sudha, R., Kalpana, K., Rajachandrasekar, T., & Arivoli, S. (2007). Comparative study on the adsorption kinetics and thermodynamics of metal ions onto acid activated low cost pandanus carbon. *E-Journal of Chemistry*, *4*(2), 238–254. https://doi.org/10.1155/2007/304305

Suresh Kumar, P., Korving, L., Keesman, K. J., van Loosdrecht, M. C. M., & Witkamp, G. J. (2019). Effect of pore size distribution and particle size of porous metal oxides on phosphate adsorption capacity and kinetics. *Chemical Engineering Journal*, *358*, 160–169. https://doi.org/10.1016/j.cej.2018.09.202

Swenson, H., & Stadie, N. P. (2019). Langmuir's Theory of Adsorption: A Centennial Review [Review-article]. *Langmuir*, *35*, 5409–5426. https://doi.org/10.1021/acs.langmuir.9b00154

Synthesis and adsorption properties of activated carbons from biomass of Prunus domestica and Jacaranda mimosifolia for the removal of heavy metals and dyes from water. (2013). *42*, 315–323. https://doi.org/10.1016/j.indcrop.2012.05.029

Thanh, N. T. K., Maclean, N., & Mahiddine, S. (2014). Mechanisms of nucleation and growth of nanoparticles in solution. *Chemical Reviews*, *114*(15), 7610–7630. https://doi.org/10.1021/cr400544s

Thurston, J. H., Hunter, N. M., Wayment, L. J., & Cornell, K. A. (2017). Urea-derived graphitic carbon nitride (u-g-C3N4) films with highly enhanced antimicrobial and sporicidal activity. *Journal of Colloid and Interface Science*, *505*, 910–918. https://doi.org/10.1016/j.jcis.2017.06.089

Usall, J., Torres, R., & Teixidó, N. (2016). Biological control of postharvest diseases on fruit: a suitable alternative? *Current Opinion in Food Science*, *11*, 51–55. https://doi.org/10.1016/j.cofs.2016.09.002

Utomo, E., Blok, B. F., Pastoor, H., Bangma, C. H., & Korfage, I. J. (2015). The measurement properties of the five-item International Index of Erectile Function (IIEF-5): A Dutch validation study. *Andrology*, *3*(6), 1154–1159. https://doi.org/10.1111/andr.12112

Vassilev, S. V., Baxter, D., Andersen, L. K., Vassileva, C. G., & Morgan, T. J. (2012). An overview of the organic and inorganic phase composition of biomass. *Fuel*, *94*, 1–33. https://doi.org/10.1016/j.fuel.2011.09.030

Vazinishayan, A., Yang, S., Lambada, D. R., Zhang, G., & Wang, Y. (2018). Investigation of the effects of tensile strain on optical properties of ZnO nanowire. *Chinese Journal of Physics*, *56*(5), 1799–1809. https://doi.org/10.1016/j.cjph.2018.07.017

Venkateswarlu, S., Lee, D., & Yoon, M. (2016). Bioinspired 2D-Carbon Flakes and Fe3O4 Nanoparticles Composite for Arsenite Removal. *ACS Applied Materials and Interfaces*, *8*(36), 23876–23885. https://doi.org/10.1021/acsami.6b03583

Viju Kumar, V. G., & Prem, A. A. (2018). Green synthesis and characterization of iron oxide nanoparticles using phyllanthus niruri extract. *Oriental Journal of Chemistry*, *34*(5), 2583–2589. https://doi.org/10.13005/ojc/340547

Vikrant, K., & Kim, K. (2018). Nanomaterials for the adsorptive treatment of Hg(II) ions from water. *Chemical Engineering Journal*, *October*. https://doi.org/10.1016/j.cej.2018.10.022

Vunain, E. (2017). Synthesis and characterization of low-cost activated carbon prepared from Malawian baobab fruit shells by H 3 PO 4 activation for removal of Cu (II) ions : equilibrium and kinetics studies. *Applied Water Science*. https://doi.org/10.1007/s13201-017-0573-x

Wang, P., Cao, M., Wang, C., Ao, Y., Hou, J., & Qian, J. (2014). Kinetics and thermodynamics of adsorption of methylene blue by a magnetic graphene-carbon nanotube composite. *Applied Surface Science*, *290*, 116–124. https://doi.org/10.1016/j.apsusc.2013.11.010

Wang, S., Guo, W., Gao, F., & Yang, R. (2017). Characterization and Pb(II) removal potential of corn straw- and municipal sludge-derived biochars. *Royal Society Open Science*, *4*(9). https://doi.org/10.1098/rsos.170402

Wang, X., Gu, L., Zhou, P., Zhu, N., Li, C., Tao, H., Wen, H., & Zhang, D. (2017). Pyrolytic temperature dependent conversion of sewage sludge to carbon catalyst and their performance in persulfate degradation of 2-Naphthol. *Chemical Engineering Journal*, *324*, 203–215. https://doi.org/10.1016/j.cej.2017.04.101

Wang, Y., Li, J., Yuan, Y., Si, Y., Xu, J., Li, M., & Peng, X. (2021a). La(OH)3 loaded magnetic nanocomposites derived from sugarcane bagasse cellulose for phosphate adsorption: Characterization, performance and mechanism. *Colloids and Surfaces A: Physicochemical and Engineering Aspects*, *626*(May), 127060.

https://doi.org/10.1016/j.colsurfa.2021.127060

Wang, Y., Li, J., Yuan, Y., Si, Y., Xu, J., Li, M., & Peng, X. (2021b). La(OH)3 loaded magnetic nanocomposites derived from sugarcane bagasse cellulose for phosphate adsorption: Characterization, performance and mechanism. *Colloids and Surfaces A: Physicochemical and Engineering Aspects*, *626*(May), 127060. https://doi.org/10.1016/j.colsurfa.2021.127060

Worch, E. (2012). Adsorption Technology in Water Treatment. In *Adsorption Technology in Water Treatment*. https://doi.org/10.1515/9783110240238

Wu, B., Fang, L., Fortner, J. D., Guan, X., & Lo, I. M. C. (2017). Highly efficient and selective phosphate removal from wastewater by magnetically recoverable La(OH)3/Fe3O4 nanocomposites. *Water Research*, *126*, 179–188. https://doi.org/10.1016/j.watres.2017.09.034

Xie, J., Wang, Z., Lu, S., Wu, D., Zhang, Z., & Kong, H. (2014). Removal and recovery of phosphate from water by lanthanum hydroxide materials. *Chemical Engineering Journal*, *254*, 163–170. https://doi.org/10.1016/j.cej.2014.05.113

Yagub, M. T., Sen, T. K., Afroze, S., & Ang, H. M. (2014). NU SC. *Advances in Colloid and Interface Science*. https://doi.org/10.1016/j.cis.2014.04.002

Yan, F., Chu, Y., Zhang, K., Zhang, F., Bhandari, N., Ruan, G., Dai, Z., Liu, Y., Zhang, Z., Kan, A. T., & Tomson, M. B. (2015). Determination of adsorption isotherm parameters with correlated errors by measurement error models. *Chemical Engineering Journal*, *281*, 921–930. https://doi.org/10.1016/j.cej.2015.07.021

Yang, H., Masse, S., Rouelle, M., Aubry, E., Li, Y., Roux, C., Journaux, Y., Li, L., & Coradin, T. (2015). Magnetically recoverable iron oxide–hydroxyapatite nanocomposites for lead removal. *International Journal of Environmental Science and Technology*, *12*(4), 1173–1182. https://doi.org/10.1007/s13762-014-0514-2

Yang, J., Chen, H., Gao, J., Yan, T., Zhou, F., Cui, S., & Bi, W. (2016). Synthesis of Fe3O4/g-C3N4 nanocomposites and their application in the photodegradation of 2,4,6-trichlorophenol under visible light. *Materials Letters*, *164*, 183–189. https://doi.org/10.1016/j.matlet.2015.10.130

Yao, H., Dai, Q., & You, Z. (2015). Fourier Transform Infrared Spectroscopy characterization of aging-related properties of original and nano-modified asphalt binders. *Construction and Building Materials*, *101*(Md), 1078–1087. https://doi.org/10.1016/j.conbuildmat.2015.10.085

Yew, Y. P., Shameli, K., Miyake, M., Kuwano, N., Bt Ahmad Khairudin, N. B., Bt Mohamad, S. E., & Lee, K. X. (2016). Green Synthesis of Magnetite (Fe3O4) Nanoparticles Using Seaweed (Kappaphycus alvarezii) Extract. *Nanoscale Research Letters*, *11*(1). https://doi.org/10.1186/s11671-016-1498-2

Yu, X., Tong, S., Ge, M., Zuo, J., Cao, C., & Song, W. (2013). One-step synthesis of magnetic composites of cellulose@iron oxide nanoparticles for arsenic removal. *Journal of Materials Chemistry A*, *1*(3), 959–965. https://doi.org/10.1039/c2ta00315e

Yuvakkumar, R., & Hong, S. I. (2014). Green synthesis of spinel magnetite iron oxide nanoparticles. *Advanced Materials Research*, *1051*, 39–42. https://doi.org/10.4028/www.scientific.net/AMR.1051.39

Zabi, N. Z., Ibrahim, W. N. W., Hanapi, N. S. M., & Hadzir, N. M. (2021). *Removal of Various Contaminants by Highly Porous Activated Carbon Sorbent Derived from Agricultural Waste Produced in Malaysia - A Review*.

Zaghbani, N., Hafiane, A., & Dhahbi, M. (2007). Separation of methylene blue from aqueous solution by micellar enhanced ultrafiltration. *Separation and Purification Technology*, *55*(1), 117–124. https://doi.org/10.1016/j.seppur.2006.11.008

Zhang, K., Zuo, W., Wang, Z., Liu, J., Li, T., Wang, B., & Yang, Z. (2015). A simple route to CoFe2O4 nanoparticles with shape and size control and their tunable peroxidase-like activity. *RSC Advances*, *5*(14), 10632–10640. https://doi.org/10.1039/c4ra15675g

Zhang, L., Zhou, Q., Liu, J., Chang, N., Wan, L., & Chen, J. (2012). Phosphate adsorption on lanthanum hydroxide-doped activated carbon fiber. *Chemical Engineering Journal*, *185–186*, 160–167. https://doi.org/10.1016/j.cej.2012.01.066

Zhang, S., Tao, L., Jiang, M., Gou, G., & Zhou, Z. (2015). Single-step synthesis of magnetic activated carbon from peanut shell. *Materials Letters*, *157*, 281–284. https://doi.org/10.1016/j.matlet.2015.05.117

Zhang, Y., Chen, B., Zhang, L., Huang, J., Chen, F., Yang, Z., Yao, J., & Zhang, Z. (2011). Controlled assembly of Fe3O4 magnetic nanoparticles on graphene oxide. *Nanoscale*, *3*(4), 1446–1450. https://doi.org/10.1039/c0nr00776e

Zhang, Y., Zhou, F., Wang, W., Guo, H., Liu, M., Zhu, H., & Sun, H. (2020). Recyclable adsorbents based on Fe3O4 nanoparticles on lanthanum-modified montmorillonite for the efficient phosphate removal. *IET Nanobiotechnology*, *14*(6), 527–536. https://doi.org/10.1049/iet-nbt.2020.0012

Zhao, W., Luo, L., Wang, H., & Fan, M. (2016). Synthesis of Bamboo-Based Activated Carbons with Super-High Specific Surface Area for Hydrogen Storage. *BioResources*, *12*(1), 1246–1262. https://doi.org/10.15376/biores.12.1.1246-1262

Zheng, D., Yao, R., Sun, C., Zheng, Y., & Liu, C. (2021). Highly Efficient Low-Concentration Phosphate Removal from Effluents by Recoverable La(OH)3/Foamed Nickel Adsorbent. *ACS Omega*, *6*(8), 5399–5407. https://doi.org/10.1021/acsomega.0c05489

Zhong, Z., Yang, Q., Li, X., Luo, K., Liu, Y., & Zeng, G. (2012). Preparation of peanut hull-based activated carbon by microwave-induced phosphoric acid activation and its application in Remazol Brilliant Blue R adsorption. *Industrial Crops & Products*, *37*(1), 178–185. https://doi.org/10.1016/j.indcrop.2011.12.015

Zhou, L., Shao, Y., Liu, J., Ye, Z., Zhang, H., Ma, J., Jia, Y., Gao, W., & Li, Y. (2014). Preparation and characterization of magnetic porous carbon microspheres for removal of methylene blue by a heterogeneous fenton reaction. *ACS Applied Materials and Interfaces*, *6*(10), 7275–7285. https://doi.org/10.1021/am500576p

Appendix

Appendix I. Results of analysis for the optimum conditions

A. **Effect of pH on MB removal**

pH	Co	Ce	% Removal
3	10	0.301	96.99
5	10	0.135	98.65
7	10	0.083	99.17
9	10	0.077	99.23
11	10	0.077	99.23

B. **Effect of adsorbent dose on MB removal**

Dose(g/L)	Co	Ce	% Removal
0.05	10	1.564	84.36
0.075	10	0.961	90.39
0.1	10	0.283	97.17
0.25	10	0.208	97.95
0.5	10	0.1894	98.11

C. **Effect of contact time on MB removal**

Contact time(min)	Co	Ce	% Removal
5	10	3.0149	69.851
10	10	1.6472	83.528
15	10	0.1899	98.101
30	10	0.3519	96.481
60	10	0.3854	96.146

D. **Effect of initial concentration on MB removal**

Initial Conce(ppm)	Ce	% Removal
10	0.027	99.73
50	0.006	99.99
100	0.037	99.96
150	0.294	99.80
200	0.570	99.72